Stability criteria for the boundary layer formed by throughflow at a horizontal surface of a porous medium : extensive version

EINDHOVEN UNIVERSITY OF TECHNOLOGY
Department of Mathematics and Computing Science

RANA 01-05
February 2001

Stability criteria for the boundary layer formed by throughflow at a horizontal surface of a porous medium: extensive version

by

C.J. van Duijn, R.A. Wooding, A. van der Ploeg

Reports on Applied and Numerical Analysis
Department of Mathematics and Computing Science
Eindhoven University of Technology
P.O. Box 513
5600 MB Eindhoven, The Netherlands
ISSN: 0926-4507

Stability criteria for the boundary layer formed by throughflow at a horizontal surface of a porous medium: extensive version

by

C.J. van Duijn[1], R.A. Wooding[2], A. van der Ploeg[3]

[1] Department of Mathematics and Computing Science, Eindhoven University of Technology, P.O. Box 513, 5600 MB Eindhoven, The Netherlands

[2]CSIRO Land and Water, GPO Box 1666, Canberra, ACT 2601, Australia

[3]MARIN, PO Box 28, 6700 AA Wageningen, The Netherlands

Upflowing salty groundwater, evaporating completely at the ground surface, leads to the buildup of a saline layer, usually with solid salt on the surface. The diffusion layer below the surface, if stable, may grow to a finite thickness at equilibrium between the upflowing solution salt and the downward diffusion. The energy method used by Homsy & Sherwood to treat the gravitational stability of the diffusion layer at equilibrium is shown to lead to a Bessel equation, and the lowest value of the lower bound to the Rayleigh number is equal to the square of the smallest root of the Bessel function J_0. However, this minimum value is reached only in a limit as the wave number of a disturbance tends to zero. Here an alternative formulation is introduced, based upon the energy method, where the linear equations of motion (Darcy's law) and continuity are combined to provide a linear "differential constraint", in place of the standard integral constraint, leading to a linear sixth-order Euler-Lagrange equation. Numerical solution by the Jacobi-Davidson method for the lowest eigenfunction indicates a lower bound for the stability curve of Rayleigh number versus wave number which is in good agreement with experiment. As in the standard energy method, this accounts for subcritical instabilities at Rayleigh numbers below the critical value according to linearised theory, which occur in the presence of the throughflow.

Both the energy method with differential constraint and linearised stability theory are applied to the developing diffusion boundary layer. When the boundary layer is thin, the profile may change rapidly by diffusion. However, with the chosen boundary conditions, an initially sharp interface at the surface is stable to small perturbations; the system becomes less stable monotonically as the thickness of the diffusion layer increases. In this situation a neutral stability curve can be calculated formally in the same way as before, but it changes with time and is interpreted as a boundary between a range of Rayleigh numbers in which the system is stable, and a range in which instability may occur. The position of that boundary moves to lower Rayleigh numbers as the thickness of the diffusion layer increases, and the wave number where the Rayleigh number is a minimum decreases with time. In the limit the wave number – Rayleigh number curve tends to that for the equilibrium boundary layer, which is evidently an asymptotic limit.

1. Introduction

Consider a semi-infinite porous medium with a horizontal upper boundary. If a uniform upflow exists within the medium and through the boundary, and if appropriate boundary conditions apply, a spatially one-dimensional boundary layer may be created and sustained by the outflow. For instance, if the surface is maintained at a temperature different from that of the medium and the saturating fluid, a thermal boundary layer is formed with an equilibrium thickness proportional to the ratio of thermal diffusivity to upflow rate. Similarly, a boundary layer is formed by a dispersing solute if the solute concentration at the boundary differs from the concentration of the solution issuing from the medium. (A thermohaline problem arises when both effects are present simultaneously, but that requires separate consideration and is not pursued here.)

Such flows may occur naturally in areas of groundwater discharge. These may be characterised by very low flow rates, leading to boundary layers of significant thickness. An upflow of warm or hot groundwater has been postulated for some shallow geothermal areas (Wooding 1960). As the surface is relatively cold, a thermal boundary layer of cool water is formed below the surface. A reversal of this situation relative to gravity may arise for *in situ* coal gasification (Sherwood & Homsy 1975), where a hot reaction surface forms at the lower horizontal boundary of a cooler permeable layer. Boundary layers are also formed in semi-arid regions containing extensive areas of groundwater discharge (Gilman & Bear 1996; Wooding, Tyler & White 1997). The groundwater contains salt. After throughflow induced by evaporation, the salt remains behind at the surface to form saline deposits (salt lakes). These salt lakes may be "dry" at the surface under the influence of evaporation, or may contain standing water (ponding), perhaps varying seasonally between the two states.

In each of these examples the fluid in the horizontal groundwater boundary-layer differs in density from the fluid in the adjacent permeable medium, and the question of the gravitational stability of the boundary layer arises. Wooding (1960) treated the case of a constant-pressure (ponded) boundary by linearised stability theory. Jones & Persichetti

(1986) applied linear analysis to a permeable layer with all combinations of boundary condition and throughflow direction. Nield (1987) obtained approximate stability criteria by variational means. Gilman & Bear (1996) treated the linearised stability of a horizontal unsaturated layer (vadoze zone) overlying a shallow water table. Wooding, Tyler & White (1997) discussed saturated groundwater movement with "dry" or ponded conditions at the surface, and used both experimental and numerical methods to simulate the unstable behaviour of a boundary layer growing from an initial salinity discontinuity at the surface, and including the margin, of a "dry" salt lake.

In an important step, Homsy & Sherwood (1975, 1976) pointed out that the presence of throughflow contributes non-symmetric (odd order) terms to the stability equations. The linear, time-independent part of the stability equations is not self-adjoint, and linear stability analysis is applicable only when the system is definitely unstable. Subcritical instabilities of finite amplitude are possible at Rayleigh numbers below the critical value derived using linear theory (Davis 1971, Straughan 1992).

In the present work we are concerned with this aspect and also with the stability of a growing boundary layer. For simplicity we consider only the dry lake case in a vertical upflow, in which we assume that a rapidly established saturated surface layer exists yielding a steady boundary condition for the salt concentration. We will employ both the energy method and the method of linearised stability.

1.1. *Stability of the equilibrium saline boundary layer*

In applying the energy method we follow two approaches. The first one is the "standard approach" as outlined, for example, by and Homsy & Sherwood (1975, 1976) or by Straughan (1992). In this approach one incorporates an integral constraint in the class of admissible perturbations, which is based on continuity and the integrated Darcy equation. The Euler-Lagrange equations with boundary conditions can be combined into a second order linear eigenvalue problem with time as a parameter. One of the goals of this paper is to demonstrate that at equilibrium, when the boundary layer has reached its large time profile of a simple exponential, this eigenvalue problem can be solved exactly in terms of Bessel functions yielding

$$R_{E_1} = 5.7832 \tag{1.1}$$

as a value of the Rayleigh number below which the system is definitely stable; $R_{E_1}^{1/2}$ is the first root of the Bessel function J_0 (Abramowitz & Stegun 1965, p. 409).

In a second approach we deviate from Homsy and Sherwood and consider a different maximum problem. Using the same functional, we replace the integral constraint with an exact differential relation which is now based on continuity and the "pointwise" Darcy equation of motion. This yields a sixth order eigenvalue problem. At equilibrium we obtain a numerical solution using the Jacobi-Davidson method (see Appendix C). With the given boundary conditions we find approximately

$$R_{E_2} = 8.590 \tag{1.2}$$

as the largest Rayleigh number below which the system is definitely stable. The close agreement of this result with the experimental and numerical results of Wooding, Tyler & White (1997) is discussed in Section 6.

Further, we consider a linearised stability analysis of the simple equilibrium boundary layer yielding a linear fourth-order eigenvalue problem. Using a power series expansion in terms of the equilibrium saturation, we find the lower eigenvalues and also the eigenfunctions. From the smallest eigenvalue we find

$$R_L = 14.35 \tag{1.3}$$

as a critical Rayleigh number above which the system is definitely unstable.

Given the physical parameters of the system a value for the Rayleigh number R_S results. This value may fall within one of three ranges -- definitely stable for $R_S \leq R_{E_i}$ (i = 1 or 2), definitely unstable for $R_S > R_L$, and possibly unstable to disturbances of finite

amplitude (leading to subcritical instabilities) when $R_{E_i} < R_S \leq R_L$. We note that (1.1) and (1.3) correspond to the asymptotic numerical results of Homsy & Sherwood (1976). They considered throughflow in a finite slab. Their asymptotic result for large dimensionless throughflow (for instance, letting the thickness of the slab become large) corresponds, after an appropriate scaling, to our formulation.

1.2. *Time dependent growth of the saline boundary layer*

Problems of fluid instability with impulsively-generated (time-dependent) base density profiles have been discussed, in particular, by Homsy (1973), who used the energy method to treat global stability of fluid layers, and Caltagirone (1980), who compared the stability behaviour using linear and energy methods and also used finite-difference computations for a horizontal porous layer with a sudden rise in surface temperature. These studies did not involve a superimposed throughflow. Generally, the linearised instability in such cases is treated as an initial-value problem, with the spatial dependence reduced to one dimension by Fourier decomposition.

Our case involves a dispersive boundary layer in an upflow, and we shall identify approximate parameter values where instability is likely to occur. Section 3 describes the profile of the growing boundary layer, which depends only upon the time parameter τ. In the early stages of development, the layer is sufficiently thin to be stabilised by the given boundary conditions. However, the monotonic increase in layer thickness with time will be accompanied by decreasing stability of the system as the influence of the boundary diminishes. This is shown in Figures 3 and 4.

Figure 3 shows a family of curves in the a, R plane, a denoting the horizontal wave number, with time τ as parameter. The curves are obtained with the energy method based on the differential constraint. For a given time $\tau > 0$, corresponding to an instantaneous state of the growing boundary layer, let $R_E(\tau)$ denote the minimum of the corresponding curves. Similarly, Figure 4 shows a family of curves obtained with the linearised stability method. Now, let $R_L(\tau)$ denote the minimum of the curve corresponding to time τ.

We now have the following refinement with respect to the equilibrium case. If $R_S \le R_E(\infty) = R_{E_2}$, the layer will attain a stable equilibrium profile. If, however, $R_S > R_{E_2}$ we can determine a time τ_E, corresponding to $R_S = R_E(\tau_E)$, and conclude the stability of the growing boundary layer for $\tau < \tau_E$.. On the other hand, if $R_s > R_L$ we can nominate an elapsed time τ_L corresponding to $R_S = R_L(\tau_L)$ and conclude the instability of the layer for $\tau > \tau_L$. The observations follow from the nature of the curves in Figures 3 and 4. The curves in Figure 3 are upper bounds for regions of stable (a, R) combinations, whereas the curves in Figure 4 are lower bounds for regions of unstable (a, R) combinations.

We should note that the actual time of appearance of a growing instability depends substantially upon the amplitude and other properties of the perturbations present during the unstable period. The wave number selected by a growing instability tends to decrease with time due to the increasing scale of the boundary-layer thickness. It follows that the wave number determined by the crossover at $\tau = \tau_L$ should provide an upper bound to observed wave numbers.

The relationship of these theoretical and numerical calculations to the experimental and numerical results of Wooding, Tyler & White (1997) is discussed in Section 6, with Figure 5.

2. Equations for salt transport

Following earlier work (Wooding, Tyler & White 1997), we consider a uniform isotropic porous medium, neglecting compressibility and thermal effects, and examine the effects of salinity variations only. The medium is saturated (pores completely filled) with a fluid of variable density (water with dissolved salt). We denote the water density by ρ_0, the density of the fluid in 'natural circumstances' (i.e. far away from outflow boundary) by ρ_r and the local fluid density by ρ. Finally, let ρ_m be the maximum density at the outflow boundary. This number may represent the fluid density in an overlying pond or the density of the salt saturated solution. Clearly, $\rho_o < \rho_r < \rho_m$ and $\rho_r \le \rho \le \rho_m$. The movement of saline water

is governed by the fluid and salt mass-balance equations, the equation of state and Darcy's law; see for instance Hassanizadeh & Leijnse (1988).

Assuming the porosity ϕ to be constant, the fluid mass-balance equation has the form

$$\phi\frac{\partial\rho}{\partial t}+\nabla\cdot(\rho\boldsymbol{q})=0, \tag{2.1}$$

where $\boldsymbol{q}$ is the Darcy volume flow rate and t is time. With an assumed Fickian dispersive flux, the mass balance of salt reads

$$\phi\frac{\partial(\rho\omega)}{\partial t}+\nabla\cdot(\rho\omega\boldsymbol{q}-\rho D\nabla\omega)=0, \tag{2.2}$$

where ω is the mass fraction of salt (i.e. salt mass per unit volume of fluid/total mass of a unit volume of fluid) and (upright) D denotes an appropriately-defined diffusivity or dispersivity. The equation of state is taken to be, see Van Duijn, Peletier & Schotting (1993),

$$\rho=\rho_0 e^{\alpha\omega}, \tag{2.3}$$

in which the coefficient α is a constant, and finally Darcy's law is assumed to have its usual form

$$\frac{\mu}{k}\boldsymbol{q}+\nabla(p-g\rho_r z^*)-(\rho-\rho_r)g\mathbf{k}=0 \tag{2.4}$$

where p is pressure, g denotes acceleration gravity, k is medium permeability and μ is fluid viscosity. Further, z^* is the (dimensioned) depth and the dimensionless unit vector $\mathbf{k}$ is directed vertically downwards. Throughout we assume that all fluid and rock properties, except the fluid density, are constant. Combining (2.1) and (2.2) gives

$$\phi\rho\frac{\partial\omega}{\partial t}+\rho\boldsymbol{q}\cdot\nabla\omega-\nabla\cdot(D\rho\nabla\omega)=0 \tag{2.5}$$

and using the equation of state (2.3) leads to

$$\phi\frac{\partial \rho}{\partial t}+\boldsymbol{q}\cdot\nabla\rho-D\Delta\rho=0. \tag{2.6}$$

where Δ denotes the Laplacian ∇^2.

We shall now consider the approximate salt-transport equations obtained by replacing (2.1) with the incompressibility condition

$$\nabla\cdot\boldsymbol{q}=0 \tag{2.7}$$

and combining this with equations (2.4) and (2.6). Equation (2.7) is justified as follows. Introduce the saturation

$$S=\frac{\rho-\rho_r}{\rho_m-\rho_r} \quad \text{with} \quad 0\le S\le 1. \tag{2.8}$$

Substituting it into the fluid mass-balance equation (2.1) yields

$$\phi\frac{\partial S}{\partial t}+\nabla\cdot(S\boldsymbol{q})+\frac{\rho_r}{\rho_m-\rho_r}\nabla\cdot\boldsymbol{q}=0. \tag{2.9}$$

Now assuming $(\rho_m-\rho_r)/\rho_r \ll 1$, we find to leading order the incompressibility equation (2.7). This limit process was studied in detail by Van Duijn, Peletier & Schotting (1993) for a particular flow problem.

3. Problem formulation

We can define a dimensionless vector $\boldsymbol{U}$ proportional to volume flow rate from

$$\boldsymbol{U}=\frac{\boldsymbol{q}}{u_c};\quad u_c=\frac{(\rho_m-\rho_r)gk}{\mu}, \tag{3.1}$$

where u_c is the scale for gravitational convective flow rate. We choose dimensionless Cartesian coordinates (x, y, z) with origin in the surface and z directed vertically downwards. These are scaled to the thickness of the equilibrium boundary layer, $\delta = D/\varepsilon$, where ε is the rate of throughflow. The corresponding scale for dimensionless time τ is $\phi D/\varepsilon^2$. Then the non-dimensionalised forms of equations (2.7), (2.4) and (2.6) are

$$\nabla \cdot \boldsymbol{U} = 0, \tag{3.3}$$

$$\nabla P - S\mathbf{k} + \boldsymbol{U} = 0, \tag{3.3}$$

$$\frac{\partial S}{\partial \tau} + R_S \boldsymbol{U} \cdot \nabla S = \Delta S. \tag{3.4}$$

Here $P = (p - \rho_r g \delta z)/(\rho_m - \rho_r) g\delta$ represents departures of the dimensionless pressure from hydrostatic conditions. Equation (3.4) involves the Rayleigh number $R_S = (\rho_m - \rho_r) gk / \mu\varepsilon$ as dictated by the physical parameters of the system. It can be written equivalently as

$$R_S = \frac{u_c \delta}{D} = \frac{u_c}{\varepsilon} = \frac{\delta}{l}, \tag{3.5}$$

where $l = D/u_c$, the "diffusion thickness", is an intrinsic length scale. In the second form R_S is specified as the ratio of two velocities, without involving D.

Equations (3.2) - (3.4) are to be solved in the three dimensional half space $\Omega = \{(x, y, z): \ -\infty < x, y < \infty, \ z > 0\}$. Along the upper boundary we prescribe the saturation and flow corresponding to a "dry lake bed", with a sufficient rate of evaporation to remove all free surface water, and a rapid buildup of salt at the surface so that saturation is reached for $\tau \approx 0$, close to the starting time of the flow process. Further, we write $\boldsymbol{U} = \boldsymbol{U}_0$ for the assumed constant dimensionless upflow, which satisfies (3.2). This means that

$$S(x,y,0,\tau)=1 \tag{3.6}$$

and

$$\boldsymbol{U}(x,y,0,\tau)=\boldsymbol{U}_0=-\frac{\varepsilon}{u_c}\mathbf{k}=-\frac{1}{R_S}\mathbf{k} \tag{3.7}$$

for all $-\infty<x,y<\infty$ and $\tau>0$. We will investigate the stability of the solution that corresponds to the "natural" initial state in which the scaled saturation is zero: i.e.

$$S|_{\tau=0}=0 \text{ in } \Omega. \tag{3.8}$$

3.1. The primary profile

The solution of (3.2) - (3.8) is called the primary profile. Assuming $S=S(z,\tau)$ only, and taking $\boldsymbol{U}(x,y,z,\tau)=\boldsymbol{U}_0$ in Ω and for all $\tau>0$, we find that the saturation equation reduces to

$$\frac{\partial S}{\partial \tau}-\frac{\partial S}{\partial z}-\frac{\partial^2 S}{\partial z^2}=0 \quad \text{for} \quad 0<z<\infty, \tau>0. \tag{3.9}$$

The solution of this equation subject to the initial - boundary conditions (3.6), (3.8) is well-known:

$$S(\tau,z)=S_0(\tau,z)=\tfrac{1}{2}e^{-z}\operatorname{erfc}\left[\frac{z-\tau}{2\tau^{1/2}}\right]+\tfrac{1}{2}\operatorname{erfc}\left[\frac{z+\tau}{2\tau^{1/2}}\right], \tag{3.10}$$

giving

$$S_0(\tau,z)\to e^{-z}, \tag{3.11}$$

the steady-state form, as $\tau \to \infty$. The corresponding primary pressure $P = P_0$ is found by integrating Darcy's law (3.3).

In the analysis carried out in the next Sections, we drop the subscript s on R_S and simply denote the Rayleigh number by R. This is to distinguish between R as eigenvalues in the analysis and its value R_S for an actual physical system.

4. Perturbation equations and variational analysis

To investigate the stability of the primary profile given in Section 3 we follow the accustomed path and set $S = S_0 + s$, $\boldsymbol{U} = \boldsymbol{U}_0 + \boldsymbol{u}$, with $\boldsymbol{u} \equiv (u, v, w)$, and $P = P_0 + p$. Here the lower case variables denote perturbations with respect to the unperturbed upflow. Substitution of these perturbation expansions into equations (3.2) - (3.4) and writing R instead of R_S yields the system (in Ω and for $\tau > 0$)

$$\frac{\partial s}{\partial \tau} - \frac{\partial s}{\partial z} + Rw\frac{\partial S_0}{\partial z} + R\boldsymbol{u}\cdot\nabla s = \Delta s, \tag{4.1}$$

$$\nabla \cdot \boldsymbol{u} = 0, \tag{4.2}$$

$$\nabla p - s\mathbf{k} + \boldsymbol{u} = 0. \tag{4.3}$$

As in Lapwood (1948) we note that equations (4.2) and (4.3) can be combined to give for s and w the linear relation

$$\Delta w = \Delta_3 s \quad \text{in } \Omega, \tag{4.4}$$

where Δ_3 denotes the horizontal Laplacian $\partial^2/\partial x^2 + \partial^2/\partial y^2$. This expression will play a crucial role in the stability analysis carried out in Sections 4.3 and 5.

On the basis of experimental observations of early instabilities, we assume that the perturbations are periodic in the horizontal x, y - plane and satisfy homogeneous conditions along the outflow boundary and at large depth. In particular,

$$s = w = 0 \quad \text{at} \quad z = 0, \infty . \tag{4.5}$$

Because of the assumed x, y periodicity, we may restrict the analysis of the perturbation equations to the periodicity cell V, given by

$$V = \{(x, y, z):\ |x| < \pi / a_x, |y| < \pi / a_y, 0 < z < \infty\}. \tag{4.6}$$

Here a_x and a_y are the, as yet unspecified, horizontal wave numbers. We call

$$a := (a_x^2 + a_y^2)^{1/2} \tag{4.7}$$

the horizontal wave number of the periodicity cell V.

4.1. The energy method

In the energy method one estimates the time derivative of the L^2 - norm of the saturation perturbation. In particular, the aim is to find the largest Rayleigh number for which

$$\frac{d}{d\tau} \int_V s^2 < 0 \quad \text{for all} \quad \tau > 0. \tag{4.8}$$

The value of R for which this inequality is satisfied clearly will depend on the wave number a and, because $S_0 = S_0(z, \tau)$, on time τ. Once (4.8) is established, which often implies the asymptotic stability

$$\int_V s^2 \to 0 \text{ as } \tau \to \infty, \tag{4.9}$$

it follows that the L^2 - norm of the velocity perturbation is bounded or vanishes as well. This is a direct consequence of (4.2) and (4.3). Multiplying (4.3) by $\boldsymbol{u}$, integrating the result over V and using (4.2) yields

$$0 = \int_V sw - \int_V |\boldsymbol{u}|^2 . \tag{4.10}$$

Using the inequality $sw \le \frac{1}{2}s^2 + \frac{1}{2}w^2$ we find

$$\int_V |\boldsymbol{u}|^2 \le \tfrac{1}{2}\int_V s^2 + \tfrac{1}{2}\int_V w^2 \le \tfrac{1}{2}\int_V s^2 + \tfrac{1}{2}\int |\boldsymbol{u}|^2 .$$

Thus

$$\int_V |\boldsymbol{u}|^2 \le \int_V s^2 , \tag{4.11}$$

which proves the assertion. To investigate (4.8) we multiply (4.1) by s and integrate over V. Using again (4.2) we find the identity

$$\frac{d}{d\tau}\tfrac{1}{2}\int_V s^2 = -\int_V |\nabla s|^2 - R\int_V sw\frac{\partial S_0}{\partial z} . \tag{4.12}$$

Thus if R is chosen such that the right-hand side of (4.12) is negative for all perturbations satisfying a given constraint, then stability is guaranteed.

It is our aim to investigate the consequences of two different constraints. In the first we consider perturbations satisfying (4.2) and (4.10), which is the integrated Darcy equation. This approach is a modification of that used by Homsy & Sherwood (1976). While they considered a stationary primary profile only and solved the corresponding eigenvalue problem numerically, we are in a position to deal with the time evolution of the primary profile as well. However, we shall not pursue the time dependence for this constraint. Instead we give a complete analytical treatment of the case when the primary profile is given by (3.11) for all

$\tau > 0$. This analysis explains quite elegantly some of the previously obtained numerical results.

In the second constraint, we consider perturbations satisfying the differential (pointwise) expression (4.4). We shall treat the time dependent primary profile and show that this differential constraint significantly improves the abovementioned integral constraint.

4.2. Energy method with integral condition

In Homsy's approach (see also Straughan 1992) one combines (4.10) and (4.12) into a single expression. Multiplying the integral constraint (4.10) by R, and (4.12) by a coupling factor $\lambda^2(>0)$, one finds, with $E = \frac{1}{2}\lambda^2 \int_V s^2$,

$$\frac{dE}{d\tau} = -R\lambda^2 \int_V sw \frac{\partial S_0}{\partial z} - \lambda^2 \int_V |\nabla s|^2 + R \int_V sw - R \int_V |\boldsymbol{u}|^2.$$

Redefining the variables according to

$$\mathrm{u} = \sqrt{R}\mathrm{u} \quad \text{and} \quad s = \lambda s,$$

leads to the expression

$$\frac{dE}{d\tau} = R^{1/2} \int_V \left(\frac{1}{\lambda} - \lambda \frac{\partial S_0}{\partial z} \right) sw - \int_V |\nabla s|^2 - \int_V |\boldsymbol{u}|^2, \tag{4.13}$$

where now $E = \frac{1}{2}\int_V s^2$. This expression is almost identical to the one given by Homsy and Sherwood (1976). The only (and non-trivial) differences are in the primary density profile and in V; they consider throughflow in a finite slab with a steady primary density profile. The

object is now to find $R > 0$ such that the right hand side of (4.13) is negative for a class of admissible perturbations. This yields the maximum problem:

$$\frac{1}{R^{1/2}} = \sup_{s,\boldsymbol{u} \in H} \frac{\int_V \left(\frac{1}{\lambda} - \lambda \frac{\partial S_0}{\partial z} \right)}{\int_V |\nabla s|^2 + \int_V |\boldsymbol{u}|^2} \tag{4.14}$$

where $H = \{s, \boldsymbol{u} : x, y$ periodic with respect to V, $s, \boldsymbol{u} = 0$ at $z = 0, \infty$ and $\nabla \cdot \boldsymbol{u} = 0\}$.

The Euler-Lagrange equations corresponding to this maximum problem together with the homogeneous boundary conditions form an eigenvalue problem with $R^{1/2}$ being the eigenvalue. In view of (4.14) one considers only the smallest eigenvalue which is maximised with respect to λ.

4.2.1. An equivalent formulation

In a slightly modified approach, we return to (4.12) with (4.10) and consider the maximum problem

$$\frac{1}{R} = \sup_{s,\boldsymbol{u} \in H} \frac{-\int_V \frac{\partial S_0}{\partial z} sw}{\int_V |\nabla s|^2} \tag{4.15}$$

with

$H = \{s, \boldsymbol{u}$: x, y periodic with respect to V, $s, \boldsymbol{u} = 0$ at $z = 0, \infty$ and $\nabla \cdot \boldsymbol{u} = 0$, $\int_V |\boldsymbol{u}|^2 = \int_V sw\}$.

The Euler-Lagrange equations follow from the first variation of the functional

$$J(s,\boldsymbol{u}) = \int_V |\nabla s|^2 + R \int_V \frac{\partial S_0}{\partial z} sw + \mu \int_V \{|\boldsymbol{u}|^2 - sw\} + \int_V \pi \nabla \cdot \boldsymbol{u} \quad , \tag{4.16}$$

where μ (constant in space) and π are Lagrange multipliers. As a result we find

$$\begin{cases} -2\Delta s + R\dfrac{\partial S_0}{\partial z} w - \mu w = 0, \\ 2\mu \boldsymbol{u} - \nabla\pi + R\dfrac{\partial S_0}{\partial z} s\mathbf{k} - \mu s\mathbf{k} = 0, \\ \nabla \cdot \boldsymbol{u} = 0 \quad \text{and} \quad \displaystyle\int_V |\boldsymbol{u}|^2 = \int_V sw. \end{cases}$$

Applying the scaling

$$\boldsymbol{u} := \frac{\lambda}{R^{1/2}}\boldsymbol{u}, \quad \mu = \frac{R}{\lambda^2} \quad \text{and} \quad p = -\tfrac{1}{2}\frac{\lambda}{R^{1/2}}\pi,$$

one finds

$$\begin{cases} \dfrac{R^{1/2}}{2}\left(\dfrac{1}{\lambda} - \lambda\dfrac{\partial S_0}{\partial z}\right) w + \Delta s = 0, & (4.17) \\ \dfrac{R^{1/2}}{2}\left(\dfrac{1}{\lambda} - \lambda\dfrac{\partial S_0}{\partial z}\right) s\mathbf{k} - \boldsymbol{u} - \nabla p = 0, & (4.18) \\ \nabla \cdot \boldsymbol{u} = 0, & (4.19) \\ \displaystyle\int_V |\boldsymbol{u}|^2 = \frac{R^{1/2}}{\lambda}\int_V sw. & (4.20) \end{cases}$$

Equations (4.17) - (4.19) were also found by Homsy & Sherwood, and indeed also arise as the Euler-Lagrange equations of the maximum problem (4.14). However, here the parameter λ is fixed by the additional constraint (4.20). Later we show, see Figure 1, that this choice maximises the eigenvalue $R^{1/2}$. Note also that (4.18) has a structure similar to Darcy's law.

As before, (4.18) and (4.19) can be combined to give

$$\Delta w = \frac{R^{1/2}}{2}\left(\frac{1}{\lambda} - \lambda\frac{\partial S_0}{\partial z}\right)\Delta_3 s. \qquad (4.21)$$

Further, multiplying (4.18) by $\boldsymbol{u}$, integrating the result over V, and using (4.20) yields the useful identity

$$\lambda^2 = \frac{\int_V sw}{-\int_V \frac{\partial S_0}{\partial z} sw}. \tag{4.22}$$

Finally, multiplying (4.17) by s, integrating the result over V, and using (4.22) gives

$$\int_V |\nabla s|^2 = \frac{R^{1/2}}{\lambda} \int_V sw. \tag{4.23}$$

Next we introduce the periodicity. Setting $s := as$, with a given by (4.7), we find from (4.17) and (4.21) the equations (with D signifying d/dz)

$$(D^2 - a^2)s + \frac{aR^{1/2}}{2}\left(\frac{1}{\lambda} - \lambda \frac{\partial S_0}{\partial z}\right) w = 0, \tag{4.24}$$

$$(D^2 - a^2)w + \frac{aR^{1/2}}{2}\left(\frac{1}{\lambda} - \lambda \frac{\partial S_0}{\partial z}\right) s = 0, \tag{4.25}$$

for $0 < z < \infty$. Note that in these equations τ appears as a parameter through the primary profile. We seek non-trivial solutions subject to the homogeneous boundary conditions (4.6) and the constraint (4.22).

As a first observation we note that (4.24), (4.25) and the boundary conditions imply $s = w$. Hence we are left with the second order boundary value problem

$$\begin{cases} (D^2 - a^2)s + \frac{aR^{1/2}}{2}\left(\frac{1}{\lambda} - \lambda \frac{\partial S_0}{\partial z}\right) s = 0 \qquad 0 < z < \infty, & (4.26) \\ s(0) = s(\infty) = 0, & (4.27) \end{cases}$$

subject to the constraint

$$\lambda^2 = \frac{\int_0^\infty s^2}{-\int_0^\infty \frac{\partial S_0}{\partial z} s^2}. \tag{4.28}$$

Identity (4.23) rewrites into

$$\int_0^\infty (Ds)^2 = \left(\frac{R^{1/2} a}{\lambda} - a^2 \right) \int_0^\infty s^2 \tag{4.29}$$

This expression and equation (4.26), using $\frac{\partial S_0}{\partial z} \to 0$ as $z \to \infty$, imply that nontrivial solutions exist only in the parameter range

$$1 < \frac{R^{1/2}}{a\lambda} < 2. \tag{4.30}$$

In the analysis below we confine ourselves to the equilibrium case (3.11), where S_0 is a simple decaying exponential.

Introducing the new parameters

$$\delta = \frac{R^{1/2}}{a\lambda} \text{ (with } 1 < \delta < 2), \quad \alpha = \left(\frac{2R}{\delta} \right)^{1/2} \text{ and } \quad \beta = \beta(a,\delta) = 2a\sqrt{1 - \frac{\delta}{2}}, \tag{4.31}$$

and the transformation

$$\xi = \alpha e^{-z}, \quad f(\xi) = s(z), \tag{4.32}$$

we find for f a boundary value problem involving the Bessel equation

$$\xi^2 f'' + \xi f' + (\xi^2 - \beta^2) f = 0 \quad \text{on} \quad 0 < \xi < \alpha, \tag{4.33}$$

with

$$f(0) = f(\alpha) = 0, \tag{4.34}$$

where each prime signifies $d/d\xi$. A solution of (4.33) satisfying the first condition in (4.34) is

$$f(\xi) = \mathrm{J}_\beta(\xi), \tag{4.35}$$

with J_β denoting the Bessel function of the first kind, order β.

Next we fix $a > 0$ and consider

$$J_{\beta(a,\delta)}(\xi_1) = 0 \quad \text{for} \quad 1 < \delta < 2, \tag{4.36}$$

where $\xi_1 = \xi_1(a,\delta)$ is the first positive zero of J_β. Then setting $\alpha = \xi_1$ in the second equation of (4.31), we obtain the first eigenvalue R_1 for the given values of a and δ:

$$R_1 = R_1(a,\delta) = \tfrac{1}{2}\delta(\xi_1(a,\delta))^2 \quad \text{for} \quad 1 < \delta < 2. \tag{4.37}$$

Keeping a fixed, we now turn to the integral constraint (4.30). In the transformed variables it reads

$$\frac{1}{\delta} = 2a^2 \frac{\int_0^{\xi_1} \frac{1}{\xi} J_\beta^2(\xi)\, d\xi}{\int_0^{\xi_1} \xi\, J_\beta^2(\xi)\, d\xi}. \tag{4.38}$$

.

The question now arises whether there exists a number $\delta_a \in (1,2)$ such that $\delta = \delta_a$ satisfies (4.38). We show in Appendix A that this is indeed the case for every $a > 0$. If we can determine it, then

$$R_1(a) := R_1(a, \delta_a) \quad \text{for} \quad a > 0. \tag{4.39}$$

In Figure 1, curve S shows the eigenvalue (4.37) plotted as $R_1^{1/2}$ versus the parameter λ for a given positive wave number a (= 0.759 in this example) and for the range $1 < \delta < 2$. Note that the straight lines $\delta = 1$ and $\delta = 2$ have slopes a and $2a$ respectively.

To map the effect of the constraint (4.38), we note that β and ξ_1 are related through (4.36). Selecting a value of β in the interval $(0, a\sqrt{2})$, we use the constraint to calculate a new value of $\delta = \delta_a$ say. With a still fixed, this leads to corresponding values $R_1 = R_{1a}$ and $\lambda = \lambda_a$ from (4.37) and the first of (4.31) respectively. The values (λ_a, R_{1a}) have been plotted as the short-dashed curve C in Figure 1. Evidently the constraint (4.38) is satisfied on the curve S at just two points, circled in Figure 1, and the single maximum of curve S is identified by the point of intersection with curve C.

Obviously, these curves take different forms when we vary a. However, the curves all reach the same R - value as $\delta \to 2$. Indeed, when $\delta \to 2$ then $\beta(a,\delta) \to 0$ and consequently $\xi_1(a,\delta) \to \xi_1^0$, the first zero of J_0. Hence, for all $a > 0$,

$$R_1(a,\delta) \to (\xi_1^0)^2 = 5.784... \quad \text{as} \quad \delta \to 2. \tag{4.40}$$

The value at $\delta = \delta_a$ defined in (4.39) corresponds to a higher value of $R_1(a)$ for all $a > 0$, thereby furnishing a preferable lower bound. This energy stability curve is plotted in the a, R plane as curve 1 in Figure 2 for comparison with further results from the energy method and from linearised instability theory. Homsy & Sherwood (1976) maximised R_1 with respect to λ numerically, followed by minimisation with respect to a, and found (4.40) approximately as a stability bound.

4.3. Energy method with differential condition

In another approach we consider a maximum problem based on (4.12) and (4.4). Now we seek the largest possible $R > 0$ such that the right hand side of (4.12) is negative for a class of perturbations s, w satisfying (4.4). This yields the maximum problem

$$\frac{1}{R} = \sup_{s, \boldsymbol{u} \in \tilde{H}} \frac{-\int_V \frac{\partial S_0}{\partial z} sw}{\int_V |\nabla s|^2} \tag{4.41}$$

where

$\tilde{H} = \{s, w : x, y$ periodic with respect to V, s, $w = 0$ at $z = 0, \infty$ and $\Delta w = \Delta_3 s$ in $V\}$.

This maximum problem will result in an eigenvalue problem which has a much higher complexity than the eigenvalue problem related to (4.15). In fact it leads to a sixth order differential equation in terms of w, for which no explicit solution is known. However, one expects to have a more accurate description, yielding larger Rayleigh numbers, in particular since now Darcy's law is accounted for exactly in the class of admissible perturbations.

4.3.1 The Euler Lagrange equations

To simplify the analysis we first formulate (4.41) in terms of x, y periodic functions. This yields

$$\frac{1}{R} = \sup_{s,w \in \tilde{H}_z} \frac{-\int_0^\infty \frac{\partial S_0}{\partial z} swdz}{\int_0^\infty \left\{(Ds)^2 + a^2 s^2\right\} dz} \tag{4.42}$$

where now

$$\tilde{H}_z = \left\{s, w: s, w = 0 \text{ at } z = 0, \infty \text{ and } \left(D^2 - a^2\right)w = -a^2 s \text{ on } (0,\infty)\right\}.$$

Proceeding as usual we consider the functional

$$J = \int_0^\infty \{(Ds)^2 + a^2 s^2\} + R\int_0^\infty \frac{\partial S_0}{\partial z} sw + \int_0^\infty \pi\{(D^2 - a^2)w + a^2 s\} \tag{4.43}$$

where π is the Lagrange multiplier. The first variation reads (with $s = s + \varphi$, $w = w + \psi$)

$$\delta J = 2\int_0^\infty \{DsD\varphi + a^2 s\varphi\} + R\int_0^\infty \frac{\partial S_0}{\partial z}\{s\psi + w\varphi\} + \int_0^\infty \pi\{(D^2 - a^2)\psi + a^2\varphi\} = 0 \tag{4.44}$$

for all φ, ψ satisfying $\varphi(0) = \psi(0) = 0$ and φ, ψ together with all derivatives vanish as $z \to \infty$. Since φ and ψ can be varied independently we deduce from (4.44) two equations. Setting $\psi = 0$ with φ arbitrary we find

$$(D^2 - a^2)s = \frac{R}{2}\frac{\partial S_0}{\partial z} w + \frac{a^2}{2}\pi \tag{4.45}$$

Next, setting $\varphi = 0$ with ψ arbitrary we find

$$0=\int_0^\infty \left\{ R\frac{\partial S_0}{\partial z}s+(D^2-a^2)\pi \right\}\psi-\pi(0)\,D\psi(0)$$

which implies

$$(D^2-a^2)\pi=-R\frac{\partial S_0}{\partial z}s, \tag{4.46}$$

and the natural boundary condition $\pi(0)=0$. Combined with (4.45) and (4.46) we have, of course,

$$(D^2-a^2)w=-a^2 s \tag{4.47}$$

Eliminating π from equations (4.45) and (4.46) yields a fourth order equation in s and w, and the further elimination of s using (4.47) leads to the sixth order w equation

$$(D^2-a^2)^3 w+\frac{a^2R}{2}\left\{(D^2-a^2)\left(\frac{\partial S_0}{\partial z}w\right)+\frac{\partial S_0}{\partial z}(D^2-a^2)w\right\}=0, \tag{4.48}$$

The corresponding boundary conditions for this equation are

$$w(\infty)=0, \tag{4.49}$$

implying that all higher order derivatives vanish as well at $z=\infty$,and

$$w(0)=D^2w(0)=D^4w(0)=0 \tag{4.50}$$

The first two conditions are obvious. The third one is a consequence of $\pi(0)=0$; this condition implies $D^2s(0)=0$ from (4.45), which is then used in (4.47). In terms of the variables w, s and π, we have the homogeneous conditions

$$w = s = \pi = 0 \quad \text{at} \quad z = 0, \infty . \tag{4.51}$$

The eigenvalue problem (4.48), (4.49) and (4.50), or equivalently (4.45) - (4.47) subject to (4.51), was solved numerically by the Jacobi-Davidson method. This method is discussed in Appendix C.

For a given wave number $a > 0$ and time $\tau > 0$, let $R_E(a,\tau)$ denote the smallest positive eigenvalue. The dashed curves in Figure 3 show the numerical approximations of the curves $\{(a,R)\colon\ a>0,\ R = R_E(a,\tau)\}$ for increasing values of τ. Note that these curves essentially move downwards, except for large a and τ. At large time they converge to the equilibrium curve, corresponding to (3.11). This limit case is also shown in Figure 2 (curve 2). As would be expected, the results obtained with the differential constraint are superior to the results obtained with the integral constraint. In particular, the minimum of curve 2 is R = 8.590 approximately, which is significantly higher than the minimum of about R = 5.78 of curve 1.

To interpret the results of the time dependent case, we set

$$R_E(\tau) := \min_{a>0} R_E(a,\tau) =: R_E(a_{min}(\tau),\tau) \quad \text{for} \quad 0 < \tau < \infty \tag{4.52}$$

and we recall the Rayleigh number of the physical system R_S , given by (3.5).

If $R_S < R_E(\infty) =: R_E$, which we denoted by R_{E_2} in the Introduction, the boundary layer is definitely stable for all $\tau > 0$. However, if $R_S > R_E$, we can only conclude that the boundary layer is stable for $0 < \tau \le \tau_E$, where τ_E is determined by $R_S = R_E(\tau_E)$. When $\tau > \tau_E$ no direct conclusions can be drawn.

The curve connecting the minima, i.e. $\{(a,R)\colon\ a = a_{min}(\tau), R = R_E(\tau) \text{ with } \tau > 0\}$, is shown as a dashed curve in Figure 3. This curve is also discussed in connection with experimental and other numerical results in Section 6 (Figure 5).

4.3.2. The case of zero throughflow

Although we are concerned primarily with the saline boundary layer, we note here the classical stability problem of a horizontal porous layer of finite depth, without throughflow, in which the base profile S is time independent and linearly decreasing downwards through the range (0,1) in z. This is included in the studies of Homsy & Sherwood (1975, 1976), and corresponds to the case $\gamma \to 0$ in their notation. Let

$$\frac{\partial S_0}{\partial z} = -k \qquad k > 0 \tag{4.53}$$

where k^{-1} is the dimensionless depth of the porous layer. If the dimensioned layer depth is chosen as the appropriate length scale, then obviously $k = 1$. With the modified profile, the Euler-Lagrange equations (4.45)-(4.47) become

$$\begin{cases} (D^2 - a^2)s = \kappa(\pi - kw), \\ (D^2 - a^2)\pi = \kappa k s, \\ (D^2 - a^2)w = -\kappa s, \end{cases} \tag{4.54}$$

where we used the transformations $w := a^2\overline{w}$, $\pi = R\overline{\pi}$ and $s := \kappa\overline{s}$ with $\kappa^2 = \frac{a^2 R}{2}$, and then dropped the overbar.

Since π and w share the same homogeneous boundary conditions, the last two equations of (4.54) give $\pi = -kw$. Then (4.54) reduces to the two equations

$$\begin{cases} (D^2 - a^2)s = -2\kappa k w, \\ (D^2 - a^2)w = -\kappa s. \end{cases}$$

Introducing the additional scaling $w = \alpha\overline{w}$ and dropping the overbar again gives

$$\begin{cases} (D^2 - a^2)s = -2\alpha\kappa k w, \\ (D^2 - a^2)w = -\dfrac{\kappa}{\alpha} s. \end{cases}$$

Now if we choose $\dfrac{\kappa}{\alpha} = 2\alpha\kappa k$ which implies $\alpha = \dfrac{1}{\sqrt{2k}}$, we find $s = w$. Hence the eigenvalue problem reduces to

$$\begin{cases} (D^2 - a^2)s = -\kappa\sqrt{2k}\, s & 0 < z < 1, \\ s(0) = s(1) = 0. \end{cases} \tag{4.55}$$

If $n = 1, 2, \ldots$, the eigenvalues κ_n are given by

$$\kappa_n = \frac{a^2 + n^2\pi^2}{\sqrt{2k}}, \tag{4.56}$$

and in terms of the Rayleigh number,

$$R_n = \frac{1}{k}\frac{(a^2 + n^2\pi^2)^2}{a^2}. \tag{4.57}$$

The same well-known result is obtained using linearised stability theory (Lapwood 1948), or by using the integral constraint (Homsy & Sherwood 1975, 1976). In this case, in fact, the problem is self-adjoint and subcritical instabilities cannot occur.

5. Linearised stability analysis and time dependence

In the method of linearised stability one disregards the higher order terms in (4.1) and considers the approximate linear saturation equation

$$\frac{\partial s}{\partial \tau} - \frac{\partial s}{\partial z} + Rw\frac{\partial S_0}{\partial z} = \Delta s \text{ in } \Omega \tag{5.1}$$

for $\tau > 0$. We shall seek nontrivial solutions of this equation together with (4.4), subject to the homogeneous boundary conditions (4.6). In case of a stationary primary profile one looks for solutions having an exponential growth rate in time. Since here, the primary profile depends on time as well, such a construction is only possible under the assumption that the rate of change of the primary profile is small compared with the growth rate of infinitesimal perturbations. Hence, for given $\tau > 0$, we consider instead of (5.1) the approximate equation

$$\frac{\partial s}{\partial \tau'} - \frac{\partial s}{\partial z} + Rw\frac{\partial S_0}{\partial z}(\tau, z) = \Delta s \text{ in } \Omega \tag{5.2}$$

for $\tau' > 0$ and sufficiently small. Now again τ appears as a parameter in the equation, as in the case of the energy methods. Applying again the x, y periodicity, taking σ as the exponential growth rate and setting

$$s, w = s, w(z)\ \exp\{\sigma\tau' + i(a_x x + a_y y)\}, \tag{5.3}$$

we find from (4.4) and (5.2) the coupled set of second order equations

$$\left(D^2 - a^2\right)w = -a^2 s, \tag{5.4}$$

and

$$\left(D^2 + D - a^2 - \sigma\right)s = R\frac{\partial S_0}{\partial z}(z, \tau)w, \tag{5.5}$$

for $0 < z < \infty$. Elimination of s from these equations gives for w the fourth order eigenvalue problem

$$L_\sigma w := \left(D^2 + D - a^2 - \sigma\right)\left(D^2 - a^2\right)w = -a^2 R\frac{\partial S_0}{\partial z}(z, \tau)w \tag{5.6}$$

for $0 < z < \infty$, with

$$w(0) = D^2 w(0) = 0 \quad \text{and} \quad w(\infty) = 0. \tag{5.7}$$

Here again, $w(\infty) = 0$ implies that all derivatives vanish as well as $z \to \infty$.

In the next Sections we consider the equilibrium case $(\tau = \infty)$ and the time dependent case $(\tau < \infty)$ separately. Further, we compare the eigenvalues resulting from the time dependent (linear) case to those obtained from the energy method subject to the differential constraint.

5.1. The equilibrium case

With expression (3.11) for the unperturbed density profile, the w-equation to be considered is

$$L_\sigma w = a^2 \, \mathrm{Re}^{-z} \, w \quad \text{for} \quad 0 < z < \infty. \tag{5.8}$$

Solutions of this equation, satisfying $w(\infty) = 0$, decay exponentially fast as $z \to \infty$. This observation, and the fact that the right hand side contains e^{-z}, motivate us to express solutions as Frobenius expansions in terms of descending exponentials; i.e.

$$\begin{aligned} w(z) &= \sum\nolimits_{n=0}^{n=\infty} R^n \left(A_n^{(1)} e^{c_1 z} + A_n^{(2)} e^{c_2 z} \right) e^{-nz} \\ &=: A_0^{(1)} w^{(1)} + A_0^{(2)} w^{(2)}, \end{aligned} \tag{5.9}$$

say, where c_1 and c_2 are the negative roots of the indicial equation and where $A_0^{(1)}$ and $A_0^{(2)}$ are arbitrary constants. Following the usual procedure, one finds

$$c_1 = -a, \quad c_2 = -\tfrac{1}{2} - \left(\tfrac{1}{4} + a^2 + \sigma \right)^{\frac{1}{2}}, \tag{5.10}$$

and the subsequent terms of the series are determined by the recurrence relations

$$\frac{A_k^{(i)}}{A_{k-1}^{(i)}} = \frac{a^2}{\left[(c_i - k + 1)(c_i - k) - a^2 - \sigma\right]\left[(c_i - k)^2 - a^2\right]}, \tag{5.11}$$

where $i = 1, 2$ and $k = 1, 2, \ldots$

Non-trivial solutions exist provided that the constants $A_0^{(1)}$ and $A_0^{(2)}$ satisfy a characteristic relation posed by the boundary condition pair at $z = 0$. Using (5.9) to evaluate $w(0)$ and $D^2 w(0)$ we obtain two equations for these constants. The coefficients in these equations are the infinite series determined from (5.10) and (5.11). Non-trivial solutions can exist only if the determinant of the coefficients vanishes. From this condition one finds, for given $a > 0$ and $\sigma > -1/4 - a^2$, the eigenvalues $\{R_n(a;\sigma)\}_{n=1}^{\infty}$ satisfying $R_1 < R_2 < \cdots$. In Appendix B we show that

$$R_1(a;0) < R_1(a;\sigma) \quad \text{for} \quad \sigma > 0 \text{ (unstable regime)}$$

and

$$R_1(a;0) > R_1(a;\sigma) \quad \text{for} \quad \sigma < 0 \text{ (stable regime)}$$

For the purpose of the stability analysis we are therefore interested only in the neutral stability curve $R_1(a;0)$. Accordingly, we change notation; instead of $R_n(a;0)$ we write $R_n(a)$ or simply R_n and L_0 is being denoted by L. To find R_1 and the other roots of the determinant equation, we approximate the coefficients numerically and solve the resulting expression iteratively. The calculated values show no change when 10 or 15 terms of the series (5.9) and its relevant derivatives are taken. However, after truncation to 5 terms (Wooding 1960) the accuracy is satisfactory for computation of the minimum value of R_1 only.

In Figure 2, point values of the lowest eigenvalue R_1 versus wave number a have been plotted as crosses, showing excellent agreement with solid curve 3 – the numerical solution of the fourth order eigenvalue problem (5.6), (5.7) with (3.11) using the Jacobi-Davidson method (Appendix C). We find

$$R_L := \min_{a>0} R_1(a) = R_1(a_c) = 14.35 \tag{5.12}$$

with

$$a_c = 0.759 \tag{5.13}$$

approximately. These numbers, in good agreement with the numerical results of Homsy & Sherwood (1976), are characteristic of the linearised stability method.

5.2. Time dependent case

To study the instability of the growing boundary layer we turn to the eigenvalue problem (5.4), (5.5) together with boundary conditions (4.5). Clearly now, the eigenvalues depend on τ as well. For given wave number $a>0$ and time $\tau>0$, let $R_L(a,\tau)$ denote the smallest positive eigenvalue.

Because $\partial S_0/\partial z$ cannot be expressed in terms of simple decaying exponentials with τ as parameter, we do not use the semi-analytical Frobenius method to determine the curves $\{(a,R):\ a>0, R=R_L(a,\tau)\}$. Instead we employ the Jacobi-Davidson method (see Appendix C) to find accurate numerical approximations. These results are shown in Figure 4, where the dashed curves indicate $R_L(a,\tau)$ for increasing values of τ. Note again that these curves essentially move downwards, except for large a and τ. As $\tau\to\infty$ convergence towards the equilibrium curve $R_1(a)$ is attained.

As before, we set

$$R_L(\tau) := \min_{a>0} R_L(a,\tau) =: R_L(a_c(\tau),\tau) \tag{5.14}$$

The curve connecting the minima, i.e. $\{(a,R):\ a=a_c(\tau), R=R_L(\tau) \text{ with } \tau>0\}$, is shown as a short-dashed curve in Figure 4 (and also in Figure 5). The significance of this curve is the following.

If $R_S > R_L(\infty) =: R_L$, an estimate for the onset time of instability is found by the crossover time τ_L determined by $R_S = R_L(\tau_L)$. In other words, the boundary layer becomes unstable for $\tau > \tau_L$, with $a_c(\tau_L)$ as an estimate for the preferred wave number. If $R_S \approx R_L$, the boundary layer becomes unstable when it is close to its equilibrium profile. Then the preferred wave number for growing instabilities is given by (5.13).

For $R_S < R_L$ no definite statement about stability is possible. The results of this (and the previous) sections only imply that infinitesimal perturbations vanish for $R_S < R_L$. Subcritical instabilities originating from large perturbations may still grow in time. This is a consequence of the uniform upflow, implying that the operator L_σ with boundary conditions (5.7) is not self-adjoint (Homsy & Sherwood 1976).

5.3 Comparison with energy method

The numerical results obtained by the Jacobi-Davidson method show that the eigenvalues arising from the energy method with differential constraint and also from the linearised approach satisfy

(i) $R_E(a,\tau) \le R_L(a,\tau)$ for all $a,\tau > 0$;

(ii) the difference is relatively small.

The first observation is a direct consequence of the problem formulations. Multiplying the saturation equation (5.5) by s, with $\sigma = 0$, and integrating the result, gives

$$\int_0^\infty \{(Ds)^2 + a^2 s^2\} = R \int_0^\infty \frac{\partial S_0}{\partial z}\, sw \quad .$$

Hence, for any $a,\tau > 0$,

$$\frac{1}{R_L(a,\tau)} = \frac{-\int_0^\infty \frac{\partial S_0}{\partial z}(\cdot,\tau)\, s_1 w_1}{\int_0^\infty \{(Ds_1)^2 + a^2 s_1^2\}} \quad , \tag{5.15}$$

where s_1, w_1 denote the first set of eigenfunctions. Clearly they belong to the space $\tilde{H}_z$, which implies by the nature of the maximum problem

$$\frac{1}{R_L(a,\tau)} \leq \sup_{s,w\in\tilde{H}_z} \frac{-\int_0^\infty \frac{\partial S_0}{\partial z}(\cdot,\tau)\, s\, w}{\int_0^\infty \{(Ds)^2 + a^2 s^2\}} = \frac{1}{R_E(a,\tau)} \quad , \tag{5.16}$$

which proves (i).

For the observation (ii) we have only a tentative explanation. Equations (4.46) and (4.47) imply the identity

$$\int_0^\infty \left\{ -R\frac{\partial S_0}{\partial z} w + a^2 \pi \right\} s = 0 \quad . \tag{5.17}$$

Hence

$$-R\frac{\partial S_0}{\partial z} w + a^2 \pi \perp s \quad \text{in } L^2 - \text{sense} \ .$$

With this observation in mind, we write (4.45) as

$$(D^2 - a^2)\, s = R\frac{\partial S_0}{\partial z} w + \tfrac{1}{2}\left\{ -R\frac{\partial S_0}{\partial z} w + a^2 \pi \right\} \ . \tag{5.18}$$

The linearised approach gives (5.5), which we write (for $\sigma = 0$) as

$$(D^2 - a^2)\, s = R\frac{\partial S_0}{\partial z} - Ds \ . \tag{5.19}$$

Note that, also in this equation, $Ds \perp s$ in L^2 – sense. Hence both equations have a similar variational structure, possibly accounting for the relatively small difference in eigenvalues.

6. Discussion and conclusions

Using the simplified model described in the Introduction, we have formulated a stability problem involving a porous medium saturated with saline water flowing vertically upwards through a horizontal surface. The upflowing water is assumed to evaporate completely at the surface. Salt saturation is established quickly and is sustained there, with excess salt precipitated on the surface. Below the surface, a saline boundary layer grows by diffusion in the counter direction to the upflow. If this layer remains stable under gravity, an equilibrium state is reached where the salinity (or density) profile is exponential, decreasing downwards towards the ambient upflow value.

Since the surface salinity and upflow rate are both taken constant, the layer can be assumed stable provided that it is sufficiently thin; that is, it is initially stable, but will tend to become less stable monotonically as the thickness increases by diffusion/dispersion. It is reasonable to conclude that the system is least stable when the boundary layer has attained maximum thickness, which occurs at equilibrium. That case has been treated extensively in the present paper. The equilibrium boundary-layer thickness provides a length scale for the Rayleigh instability problem. If the porous medium has a lower boundary, it is assumed to be at a distance large relative to that scale.

If the system parameters are such that the equilibrium boundary layer would be unstable, and hence will not be formed, we have shown that there must be a critical time during the growth phase when the pre-equilibrium layer passes from a stable to an unstable state. Since the scale of the saline layer increases monotonically with time, the critical wave number is expected to provide only an upper bound for the wave number of the growing finite disturbance which subsequently appears. This approach has involved an extended application

of stability theory, with time treated as a parameter when it appears in the expression for the diffusing primary profile.

6.1. The equilibrium boundary layer: Energy methods

We have noted that the linearised stability problem for the saline boundary layer with upflow is non-selfadjoint (Homsy & Sherwood 1975,1976), and linearised stability analysis may be useful only in the range of wave numbers and Rayleigh numbers where the system is definitely unstable. At Rayleigh numbers below that range, subcritical instabilities of finite amplitude may exist (Davis 1971), and experimental and numerical studies (Wooding, Tyler & White 1977) confirm that this is indeed the case. For a theoretical analysis of this stability problem we have given detailed attention to the nonlinear instability equations and have applied the energy method. A "standard" approach similar to that of Homsy & Sherwood (1976), which includes the use of a coupling factor, gives expressions differing only through our assumption of a semi-infinite porous medium instead of a porous layer. This corresponds to their limiting case. If we assume horizontal periodicity of the perturbation in the usual way, the Euler-Lagrange equations reduce to a pair of second-order ordinary differential equations which are symmetric in the perturbation density and vertical velocity. The boundary conditions also obey this symmetry, and the system reduces to second order. For the equilibrium boundary layer, we have found that the solution is a Bessel function of the first kind. The lowest eigenvalue R is plotted versus periodicity wave number a in Figure 2, curve 1. As shown, the minimum value of R occurs at $a = 0$, and is equal to the square of the first root of the Bessel function J_0. This corresponds to the value of 5.77 found numerically by Homsy & Sherwood (1976) for their limiting case of a semi-infinite porous medium. Clearly that is a lower bound, and thus the existence of a stable range for finite positive R was proved by those authors.

However, in the resistive porous medium the perturbation induced velocity tends to zero with the horizontal wave number a, while the vertical diffusive damping across the boundary layer is approximately constant, effectively increasing stability, so that R should

increase indefinitely. The indication that a minimum lower bound is reached as $a \to 0$ departs from this, and also differs qualitatively from the behaviour of the linearised solution.

Use of the energy method involves an inequality, and details of the method and results obtained are not necessarily unique. Instead of the integral relation derived from the equation of continuity and Darcy's law, and linked through a coupling factor, we make direct use of the differential equation (4.4) relating density and velocity. The linearity of this equation is a consequence of the fact that the equation of motion, Darcy's law, is linear. This is found to lead to a maximum principle which is more closely connected with the original physical problem. A sixth-order Euler-Lagrange equation results, involving three boundary conditions at the surface. An alternative formulation, introducing a new Lagrange multiplier, leads to the same system in the form of three second-order ordinary differential equations.

These eigenvalue equations have been solved accurately using the Jacobi-Davidson numerical method (Appendix C). Figure 2, curve 2, shows the plot of the lowest eigenvalue R versus periodicity wave number a obtained for the equilibrium primary profile. Interestingly, this curve falls between curve 1 obtained by application of the "standard" energy method and curve 3 obtained by linearised stability theory, all three curves tending to have the same asymptotic form at high wave numbers. The shape of curve 2 is qualitatively the same as that of the linearised solution at low wave numbers, showing the expected behaviour as $a \to 0$. The minimum value for R, approximately 8.590, gives an improved estimate of the lower bound to possible instability.

6.2. The time dependent growing boundary layer

The case of the growing boundary layer has been studied by treating time τ as a parameter in the expression (3.10) for the primary profile, and choosing a sequence of increasing τ - values to follow the growth of the boundary layer. We considered two approaches. First, for each value of τ we used the energy method in its sixth order form to identify a curve in the a, R plane which represents an estimate of the upper limit of absolute stability. From the

properties of the energy method, this estimate is actually a lower bound and applies for arbitrary finite perturbations. Figure 3 shows the results obtained. In the second approach, we employed the fourth order linearised stability equations (5.6) and (5.7) in a similar way, to give solutions in the case of infinitesimal perturbations. These results are shown in Figure 4.

Figures 3 and 4 show qualitative similarities. Pairs of curves having the same τ-values are non-intersecting and qualitatively resemble curves 2 and 3 shown in Figure 2. The spacing between these pairs decreases with increasing τ. As τ increases, the curve minima in each case progress monotonically to lower (a, R)- values with the equilibrium values as the limit. At higher wave numbers, however, the R- values at minima first decrease and then increase with the increasing scale of the boundary layer thickness. The resultant curve intersections (crossovers) exhibit marked topological similarities in Figures 3 and 4.

6.3. Comparisons with laboratory and numerical experiments

Figure 5 repeats the equilibrium stability curves of Figure 2 and includes experimental measurements obtained using a tilted Hele-Shaw cell to simulate two-dimensional flow in a porous medium, with inflow of a saline solution and evaporation along part of the upper edge (Wooding, Tyler & White 1997). Experimental points are represented in Figure 5 by the symbols +, $\times$ and $*$. In the experiments, the large scale Rayleigh number Ra based on finite "aquifer" depth was greater than 10^2 times the boundary layer R-value. Numerical results are also given for a finite-difference model with the same boundary conditions which used a 256×128 mesh and a near-surface "random-noise" density perturbation of 0.01 times the total density difference. These parameters specifying noise provided quite good agreement with a wide range of experimental results (Simmons, Narayan & Wooding 1999). Points from the numerical studies are represented by open squares (Ra = 6400) and circles (Ra = 8000). Although the large scale flow in both the experimental and numerical work differed from a simple vertical upflow, a uniform evaporation rate was modelled and a saline boundary layer of uniform thickness was observed to develop. Wave numbers of initial instabilities, scaled to the equilibrium boundary layer thickness, were measured for a wide range of R-values. Previously, these observations were plotted by Wooding, Tyler & White

(1997, Figure 7) using wave numbers scaled to the diffusion thickness and therefore equivalent to a / R in the present case.

From the published experimental data, stable boundary layers were observed for R-values of 5.8, 5.6 (two experiments), and smaller R. Unstable boundary layers resulted for R-values of 5.6 (one experiment), 8.9 (two experiments), and larger R. Except for the unexplained appearance of instability in one experiment performed at R = 5.6, there was a clear separation of stable and unstable layers into two ranges. From the numerical model, with a mesh of 512 $\times$256 elements and a "random noise" perturbation of 0.005 times the total density difference, unstable boundary layers were observed for R-values of 9.8 and higher (Wooding, Tyler & White 1997, Figure 6). If the single unstable result at R = 5.6 is not included, the theoretical lower bound of 8.590 obtained using the alternative energy method is in agreement with the results of both the experimental and numerical studies.

The dashed curves in Figure 5 provide traces of the minima of the stability curves defined by the modified energy method in Figure 3 and by linearised stability analysis in Figure 4. For the data obtained by experimental and numerical simulation, either curve might be considered as an upper bound to the wave number of an instability which first appears. This is on the assumption that growth rate is zero at a critical point for stability, and a growing perturbation becomes significant when the boundary layer thickness scale has increased significantly. Clearly, however, the instabilities plotted in Figure 5 have been initiated by perturbations of small but finite amplitude, and the modified energy method provides the appropriate estimate. Three experimental points at the low-R end appear to be exceptional. These occur in a range where accurate observation becomes more difficult, and an inadvertent change of background conditions could have altered the wave number.

No instabilities at higher wave numbers, between the two dashed curves in Figure 5, have been recorded experimentally. Some have been found by numerical simulation, using a refined mesh of 512 $\times$ 256 elements, which extends the "random noise" spectrum to higher wave numbers, with a reduced amplitude. These have not been reproduced as the range of such perturbations has not been fully explored.

In general, we may conclude that the alternative formulation of the energy method has improved the quantitative and qualitative estimate of a lower bound to absolute stability, and is in agreement with experimental and numerical modelling. The comparison with results from linearised analysis yields interesting qualitative similarities, and stability properties of a growing boundary layer can be described in some detail. The above results could have applications to the theory of stability of salt lakes and the salinization of groundwater.

The experimental results discussed above were derived in a study initiated by I. White and carried out by Scott W. Tyler and P. A. Anderson between 1990 and 1992, and described previously in a different format (Wooding, Tyler & White 1997). We wish to acknowledge also the contributions made by H. I. J. te Riele and J. L. M. van Dorsselaer of CWI in Amsterdam, for their highly valued assistance in connection with the numerical computations. We are grateful to CSIRO Centre for Environmental Mechanics and CSIRO Land and Water for support to carry out the theoretical investigation.

Appendix A. Existence and uniqueness

To prove existence of δ_a such that (4.38) is satisfied, we fix $a>0$, arbitrarily chosen, and consider for $1<\delta<2$ the left and right hand sides of (4.38) separately, i.e.

$$\mathrm{LHS}(\delta)=\frac{1}{\delta} \tag{A1}$$

and

$$\mathrm{RHS}(\delta)=2a^2\frac{\int_0^{\xi_1}\frac{1}{\xi}J_\beta^2(\xi)\,d\xi}{\int_0^{\xi_1}\xi J_\beta^2(\xi)\,d\xi}\,, \tag{A2}$$

where $\beta=\beta(a,\delta)$ and $\xi_1=\xi_1(a,\delta)$ are defined in (4.31) and (4.36), respectively. Trivially, (A1) is strictly decreasing in δ such that LHS(1) = 1 and LHS(2) = $\frac{1}{2}$. Below we prove analytically that RHS(1) < 1 and RHS(2^-) = ∞. This clearly implies the existence of δ_a. Computationally, we verified the monotonicity of RHS(δ); see Figure 6, which in addition gives the uniqueness of δ_a for any $a>0$.

Behaviour as $\delta\downarrow 1$.

Set $w(\xi)=J_\beta(\xi)$ and consider the Bessel equation

$$\xi^2 w''+\xi w'+(\xi^2-\beta^2)w=0,\quad 0<\xi<\xi_1. \tag{A3}$$

Dividing by ξ and multiplying by w yields

$$\xi ww''+ww'+\xi w^2-\beta^2\frac{1}{\xi}w^2=0. \tag{A4}$$

Integrating this equation in ξ from $\xi=0$ to $\xi=\xi_1$ gives

$$\int_0^{\xi_1}\xi w^2=\beta^2\int_0^{\xi_1}\frac{1}{\xi}w^2-\int_0^{\xi_1}\xi ww'', \tag{A5}$$

for all $\beta>0$. Since

$$\int_0^{\xi_1}\xi ww''=\xi ww'\Big|_0^{\xi_1}-\int_0^{\xi_1}w'(w+\xi w')=-\int_0^{\xi_1}\xi(w')^2, \tag{A6}$$

we obtain

$$\int_0^{\xi_1} \xi w^2 > \beta^2 \int_0^{\xi_1} \frac{1}{\xi} w^2 , \tag{A7}$$

which implies RHS(1) < 1 , since $\lim_{\delta \downarrow 1} \beta^2(a,\delta) = 2a^2$.

Behaviour near $\delta = 2$.

Since $\lim_{\delta \uparrow 2} \beta(a,\delta) = 0$ and $J_0(\xi) \to 1$ as $\xi \downarrow 0$, the integrand in the numerator of (A2) is non-integrable as $\delta \uparrow 2$. Consequently, $\lim_{\delta \uparrow 2} \mathrm{RHS}(\delta) = \infty$.

We conclude this appendix by determining the behaviour of $R_1(a)$, see (4.39), as $a \downarrow 0$. Using (4.31), we rewrite (4.38) into

$$\frac{2}{\delta}\left(1 - \frac{\delta}{2}\right) = \frac{\beta^2 \int_0^{\xi_1} \frac{1}{\xi} J_\beta^2(\xi)\, d\xi}{\int_0^{\xi_1} \xi\, J_\beta^2(\xi)\, d\xi} . \tag{A8}$$

Since $a \to 0$, we need to investigate the right-hand side of this equation as $\beta \to 0$. From (A5) and (A6) we deduce

$$\frac{\beta^2 \int_0^{\xi_1} \frac{1}{\xi} J_\beta^2(\xi)\, d\xi}{\int_0^{\xi_1} \xi\, J_\beta^2(\xi)\, d\xi} = 1 - \frac{\int_0^{\xi_1} \xi\, J_\beta'^2(\xi)\, d\xi}{\int_0^{\xi_1} \xi\, J_\beta^2(\xi)\, d\xi} \to 1 - \frac{\int_0^{\xi_1^0} \xi\, J_1'^2(\xi)\, d\xi}{\int_0^{\xi_1^0} \xi\, J_0^2(\xi)\, d\xi} = 0$$

as $\beta \to 0$. Hence $\lim_{a \to 0} \delta_a = 2$.

Moreover since $\lim_{a \to 0} \xi_1(a,\delta) = \xi_1^0$, we find $\lim_{a \to 0} R_1(a) = \frac{1}{2}.2.(\xi_1^0)^2 = 5.784\ldots$.

Appendix B: Comparison of eigenvalues

Let $a > 0$ be fixed and consider the eigenvalue problem

$$(E_\sigma)\begin{cases} L_\sigma w = a^2 R e^{-z} w \ \text{ for } \ 0 < z < \infty, \\ w(0) = D^2 w(0) = 0 \ \text{ and } \ w(\infty) = 0, \end{cases}$$

where L_σ is defined in (5.6). Note that

$$L_\sigma = L_0 - \sigma(D^2 - a^2). \tag{B1}$$

We denote the eigenfunctions and eigenvalues of (E_σ) by $\{w_{n,\sigma}\}_{n=1}^{\infty}$ and $\{R_n(a;\sigma)\}_{n=1}^{\infty}$, respectively. The eigenvalues are ordered according to $R_1(a;\sigma) < R_2(a;\sigma) < \cdots$. We prove the following fundamental property:

Theorem. The smallest positive eigenvalues of Problem (E_σ) satisfy

$$R_1(a;0) < R_1(a;\sigma) \ \text{ for } \ \sigma > 0,$$

and

$$R_1(a;\sigma) < R_1(a;0) \ \text{ for } \ \sigma < 0.$$

Proof. We only show the first assertion. The proof of the second one is similar and is therefore omitted. Consider for $\sigma > 0$,

$$L_\sigma w_{1,\sigma} = a^2 R_1(a;\sigma) e^{-z} w_{1,\sigma}.$$

Using property (B1) we write this equation as

$$L_0 w_{1,\sigma} - a^2 R_1(a;0) e^{-z} w_{1,\sigma} = a^2 \{R_1(a;\sigma) - R_1(a;0)\} e^{-z} w_{1,\sigma} + \sigma (D^2 - a^2) w_{1,\sigma}.$$

Multiplying this expression by $w_{1,\sigma}$, integrating, and using the notations $w_\sigma = w_{1,\sigma}$ and $R_\sigma = R_1(a,\sigma)$, we arrive at

$$(w_\sigma, L_0 w_\sigma) - a^2 R_0 (w_\sigma, e^{-z} w_\sigma) = a^2 (R_\sigma - R_0)(w_\sigma, e^{-z} w_\sigma) - \sigma \{ \|Dw_\sigma\|_2^2 + a^2 \|w_\sigma\|_2^2 \},$$

where $(\cdot,\cdot)$ denotes the L^2 - inner product and $\|\cdot\|_2$ the induced norm. The left hand side of this expression is strictly positive, because

$$a^2 R_0 = \frac{(w_0, L_0 w_0)}{(w_0, e^{-z} w_0)} = \min_{w \in H} \frac{(w, L_0 w)}{(w, e^{-z} w)} < \frac{(w_\sigma, L_0 w_\sigma)}{(w_\sigma, e^{-z} w_\sigma)},$$

where $H = \{ w \in H^2(0,\infty)$: w satisfies boundary conditions$\}$.

Thus we obtain the inequality

$$a^2 (R_\sigma - R_0)(w_\sigma, e^{-z} w_\sigma) > \sigma \{ \|Dw_\sigma\|_2^2 + a^2 \|w_\sigma\|_2^2 \},$$

from which the assertion follows.

Appendix C: The Jacobi-Davidson method

In this section, we show briefly how the sixth order problem described by the combined system of equations (4.45), (4.46) and (4.47) can be solved numerically. The fourth order problem, described by (5.4) and (5.5), can be solved in a similar way.

After using the transformation introduced at (4.54),

$$w = a^2\overline{w}\,, \quad s = \kappa\overline{s}\,, \quad \pi = R\overline{\pi}\,, \text{ in which } \kappa^2 = \tfrac{1}{2}a^2R\,,$$

the system (4.45) – (4.47) can be written as

$$(D^2 - a^2)\overline{s} = \kappa\left(\overline{\pi} + \frac{\partial S_0(\tau,z)}{\partial z}\right)\overline{w}\,, \tag{C1}$$

$$(D^2 - a^2)\overline{\pi} = \kappa\left(-\frac{\partial S_0(\tau,z)}{\partial z}\right)\overline{s}\,, \tag{C2}$$

$$(D^2 - a^2)\overline{w} = -\kappa\,\overline{s}\,, \tag{C3}$$

for $0 < z < \infty$. The boundary conditions are given by $\overline{s} = \overline{\pi} = \overline{w} = 0$ at $z = 0$ and at $z = \infty$. We want to obtain $R = \dfrac{2\kappa_{\min}^2}{a^2}$ as a function of a for several values of τ. Here $\kappa_{\min}$ is the smallest positive eigenvalue of (C1) – (C3).

Before a numerical solution can be obtained, we have to decide how to deal with the boundary conditions at infinity. One possibility is to use a transformation $t = e^{-z}$. We have used the more direct approach in which the boundary conditions are applied at a finite value $z = z_{cut}$ instead of $z = \infty$. Here z_{cut} is chosen sufficiently large; increasing z_{cut} should not alter the results beyond the accuracy that we demand for the numerical solution. We have experimented with several values of z_{cut} to ensure that this criterion has been satisfied.

The next step is to discretise (C1) – (C3) for $0 < z < z_{cut}$. In order to keep the discretised system of equations reasonably small, we use a relatively large mesh size near $z = z_{cut}$, and an exponential refinement near $z = 0$. Suppose that we discretise at the points $z_1, z_2, \ldots, z_N$. At a given point z_i, the operator $(D^2 - a^2)$ is discretised using a standard, second-order scheme that involves only z_{i-1}, z_i and z_{i+1}. After discretisation, we obtain the following generalised eigenvalue problem

$$\begin{bmatrix} T & 0 & 0 \\ 0 & T & 0 \\ 0 & 0 & T \end{bmatrix} \begin{bmatrix} \hat{s} \\ \hat{\pi} \\ \hat{w} \end{bmatrix} = \kappa \begin{bmatrix} 0 & I & -D \\ D & 0 & 0 \\ -I & 0 & 0 \end{bmatrix} \begin{bmatrix} \hat{s} \\ \hat{\pi} \\ \hat{w} \end{bmatrix}. \tag{C4}$$

Here T is the tridiagonal matrix that represents the operator $D^2 - a^2$, I is the identity matrix, and D is the diagonal matrix with its i-th diagonal element equal to the value of $-\dfrac{\partial S_0(\tau, z)}{\partial z}$ at z_i. The $N \times 1$ vectors $\hat{s}, \hat{\pi}$ and $\hat{w}$ have as components the values of the corresponding functions in the discretisation points. For each $\hat{w}$, the vector $(0, D\hat{w}, \hat{w})$ is in the null space of the matrix in the right-hand side of (C4). Hence (C4) has N eigenvalues equal to infinity. Further, it can be shown that if κ is an eigenvalue not equal to zero, then so is $-\kappa$, and κ satisfies the generalised eigenvalue problem

$$T^3 \hat{w} = \kappa^2 (DT + TD)\hat{w}. \tag{C5}$$

We note that this equation corresponds to the sixth order w-equation (4.48).

We want to solve (C5) with the Jacobi-Davidson (JD) method (Sleijpen & van der Vorst 1996). This method can be used to solve generalised eigenvalue problems of the form $Ax = \mu Bx$. (See below.) We used the code that has been developed at the University of Utrecht and which is described by Fokkema, Sleijpen & van der Vorst (1999). The JD method is especially of interest when only a small number of eigenvalues μ is required and when the matrices A and B are large and sparse. An advantage is that the inverse of A or B is not required; hence JD can be used for very large eigenvalue problems (Nool & van der Ploeg 1997). Therefore, for our application, we could take $A = T^3$, $B = DT + TD$ and apply JD directly to (C5). However, from numerical experiments it appeared to be more efficient to apply JD to the following standard eigenvalue problem,

$$T^{-3}(DT + TD)\hat{w} = \lambda^{-2}\hat{w}. \tag{C6}$$

We emphasise that it is not necessary to construct the matrix T^{-3} explicitly; we only need the matrix-vector multiplication with T^{-3}. Since $-T$ is a tridiagonal, diagonally dominant matrix, we can easily construct the bidiagonal matrices L and U in such a way that $T = LU$ and L and U are lower- and upper-triangular respectively. Therefore, the result of the matrix-vector multiplication is available.

For completeness, we discuss briefly the basic ingredients of the Jacobi-Davidson method by further consideration of the standard eigenvalue problem $Ax = \mu x$. At the k-th step of the method, an approximate eigenvector is assumed – a combination of k vectors $v_1, v_2, \cdots, v_k$, where k is very small compared to N. If the $N \times k$ matrix whose columns are given by $v_1, v_2, \cdots, v_k$ is denoted by V_k, an approximate eigenvector can be written as $V_k s$, for 'small' vector s with k components. The search directions are made orthonormal to each other; hence $V_k{}^* V_k = I$.

Suppose that an approximate eigenvalue is given by θ. The vectors s and θ are constructed in such a way that the residual vector $r = AV_k s - \theta V_k s$ is orthogonal to the k search directions. From this requirement it follows that

$$V_k{}^* AV_k s = \theta V_k{}^* V_k s \Leftrightarrow V_k{}^* AV_k s = \theta s.$$

In this way one obtains a 'projected' eigenvalue problem, in which the size of the matrix is k. By using a proper restart technique one makes sure that k stays so small that this problem can be solved by a direct method. In our application, we are interested in the largest eigenvalue. Hence the eigenvalue of the projected system that has the largest norm is chosen as the approximate eigenvalue θ.

At each step of the algorithm a new search direction has to be constructed. Suppose that we have obtained an approximation u of the *true* eigenvector x associated with some eigenvalue μ. We assume that $\|u\| = 1$; hence $\theta = u^* Au$ is an approximation of μ. Let us define $P = uu^*$ being the orthogonal projector onto the subspace spanned by $\{u\}$ and let $I - P$ be the projector onto the orthogonal complement of span $\{u\}$, which is denoted by $u^{\perp}$.

Any vector $x \in C^n$ can be written as $x = x_1 + x_2$ with $x_1 \in \text{span}\{u\}$ and $x_2 \in u^\perp$. We normalise x such that $x = u + y$ with $y \perp u$. In the JD algorithm a correction vector $y \in u^\perp$ is constructed. The restriction of A to $u^\perp$ is given by

$$A_P = (I - P)A(I - P). \tag{C7}$$

If we rewrite (C7) and substitute the resulting expression for A into $Ax = \mu x$, we obtain

$$(A_P - \mu)y = -r + (\mu - \theta - u^* Ay)u. \tag{C8}$$

Both y and r are orthogonal to u and therefore, premultiplication of (C8) with u^* yields $\mu = \theta + u^* Ay$. Note that μ is unknown and its best approximation will be θ. In this way, we obtain as the correction equation

$$(I - P)(A - \theta I)(I - P)y = -r, \qquad u^* y = 0. \tag{C9}$$

It is sufficient to solve (C9) only approximately. This can be done by some steps of an iterative method, for example, GMRES. When an approximate solution y of (C9) has been constructed, it is made orthogonal to the previous search directions, and the new search direction v_{k+1} is taken equal to the normalisation $y / \|y\|$.

A more detailed description of the Jacobi-Davidson method, including the generalised eigenvalue problem, can be found in Sleijpen & van der Vorst (1996) and Fokkema, Sleijpen & van der Vorst (1999). Information on how to obtain the code can be obtained at the Internet address *http://www.math.uu.nl/people/bomhof/jd.html*

REFERENCES

ABRAMOWITZ, M. & STEGUN, I. A. 1972 *Handbook of Mathematical Functions.* Dover.

CALTAGIRONE, J.-P. 1980 Stability of a saturated porous layer subject to a sudden rise in surface temperature: comparison between the linear and energy methods. Quart. J. Mech. appl. Math. **33**, 47-58.

DAVIS, S. H. 1971 On the possibility of supercritical instabilities. In *Proc. IUTAM Symp. Herrenalb*, Instability of Continuous Systems, Springer-Verlag, Berlin, 222-227.

FOKKEMA, D. R., SLEIJPEN, G. L. G. & VAN DER VORST, H. A. 1999 Jacobi-Davidson style QR and QZ algorithms for the reduction of matrix pencils. *SIAM J. Sci. Comput.* **20**, 94-125.

GILMAN, A. & BEAR, J. 1996 The influence of free convection on soil salinization in arid regions. *Transport in Porous Media* **23**, 275-301.

HASSANIZADEH, S. M & LEIJNSE, T. 1988 On the modeling of brine transport in porous media. *Water Resour. Res.* **24**, 321-330.

HOMSY, G. M. 1973 Global stability of time-dependent flows: impulsively heated or cooled fluid layers. *J. Fluid Mech.* **60**, 129-139.

HOMSY, G. M. & SHERWOOD, A. E. 1975 Convective instabilities in porous media with through-flow. *Lawrence Livermore Lab. Rep.* UCRL-76539.

HOMSY, G. M. & SHERWOOD, A. E. 1976 Convective instabilities in porous media with through flow. *Amer. Inst. Chem. Engrs J.* **22**, 168-174.

JONES, M. C. & PERSICHETTI, J. M. 1986 Convective instability in packed beds with throughflow. *Amer. Inst. Chem. Engrs J.* **32**, 1555-1557.

LAPWOOD, E. R. 1948 Convection of a fluid in a porous medium. *Proc. Cambridge Phil. Soc.* **44**, 508-521.

NIELD, D. A. 1987 Convective instability in porous media with throughflow. *Amer. Inst. Chem. Engrs J.* **33**, 1222-1224.

NOOL, MARGREET & VAN DER PLOEG, A. 1997 A parallel Jacobi-Davidson method for solving generalized eigenvalue problems in linear magnetohydrodynamics. *Tech. Rep.* NM-R9733, CWI, Amsterdam, December, 1997.

SHERWOOD, A. E. & HOMSY, G. M. 1975 Convective instability during *in situ* coal gasification. *Lawrence Livermore Lab. Rep.* UCRL-51791.

SIMMONS, C. T., NARAYAN, K. A. & WOODING, R. A. 1999 On a test case for density-dependent groundwater flow and solute transport models: The salt lake problem. *Water Resources Res.*

SLEIJPEN, G. L. G. & VAN DER VORST, H. A. 1996 A Jacobi-Davidson iteration method for linear eigenvalue problems. *SIAM J. Matrix Anal. Appl.* **17(2)**, 401-425.

STRAUGHAN, B. 1992 *The Energy Method, Stability, and Nonlinear Convection.* Springer-Verlag, New York.

VAN DUIJN, C. J., PELETIER, L. A. & SCHOTTING, R. J. 1993 On the analysis of brine transport in porous media. *Eur. J. Appl. Math.* **4**, 271-302.

WOODING, R. A. 1960 Rayleigh instability of a thermal boundary layer in flow through a porous medium. *J. Fluid Mech.* **9**, 183-192.

WOODING, R. A., TYLER, S. W. & WHITE, I. 1997 Convection in groundwater below an evporating salt lake: 1. Onset of instability. *Water Resour. Res.* **33**, 1199-1217.

Figure Captions

Figure 1. With .wavenumber a given, curve S shows lower bound for first eigenvalue plotted versus λ ; curve C has been constructed using δ - values satisfying the integral constraint.

Figure 2. Comparison of estimates involving lowest eigenvalue R_1 versus wavenumber a for the equilibrium boundary layer. Curve 1: Energy method using integral constraint. Curve 2: Energy method using differential constraint. Curve 3: Linearised stability theory using Jacobi-Davidson numerical method (solid curve) and Frobenius expansions (crossed points).

Figure 3. Solid curve: Lower bound to R_1 for equilibrium boundary layer according to the energy method with differential constraint. Dashed curves: Lower bound for R_1 prior to equilibrium. Numerical values are calculated by Jacobi-Davidson method. Short-dashed curve traces minima of lower bound for R_1 with increasing $\tau > 0$.

Figure 4. Solid curve: Lowest eigenvalue R_1 for equilibrium boundary layer according to small perturbation theory. Dashed curves: Estimate of R_1 prior to equilibrium, treating time as parameter. Numerical values are calculated by Jacobi-Davidson method. Shorter-dashed curve traces minima of R_1 with increasing $\tau > 0$.

Figure 5. Comparison of theory (this paper) with experimental and numerical modelling results (Wooding, Tyler & White 1997). Solid curves 1-3 give eigenvalues R_1 versus wavenumber a for the equilibrium boundary layer (Figure 2). Curves of minima of R_1 with respect to a for $\tau > 0$ increasing to equilibrium: by modified energy method (Figure 3, short dashes), by linearised theory (Figure 4, shorter dashes). Symbols for experimental and numerical results are identified in the text.

Figure 6. Typical curves of RHS(δ) and LHS(δ) used for existence proof. In the most likely situation curves are monotone, giving a single point of intersection and hence uniqueness.

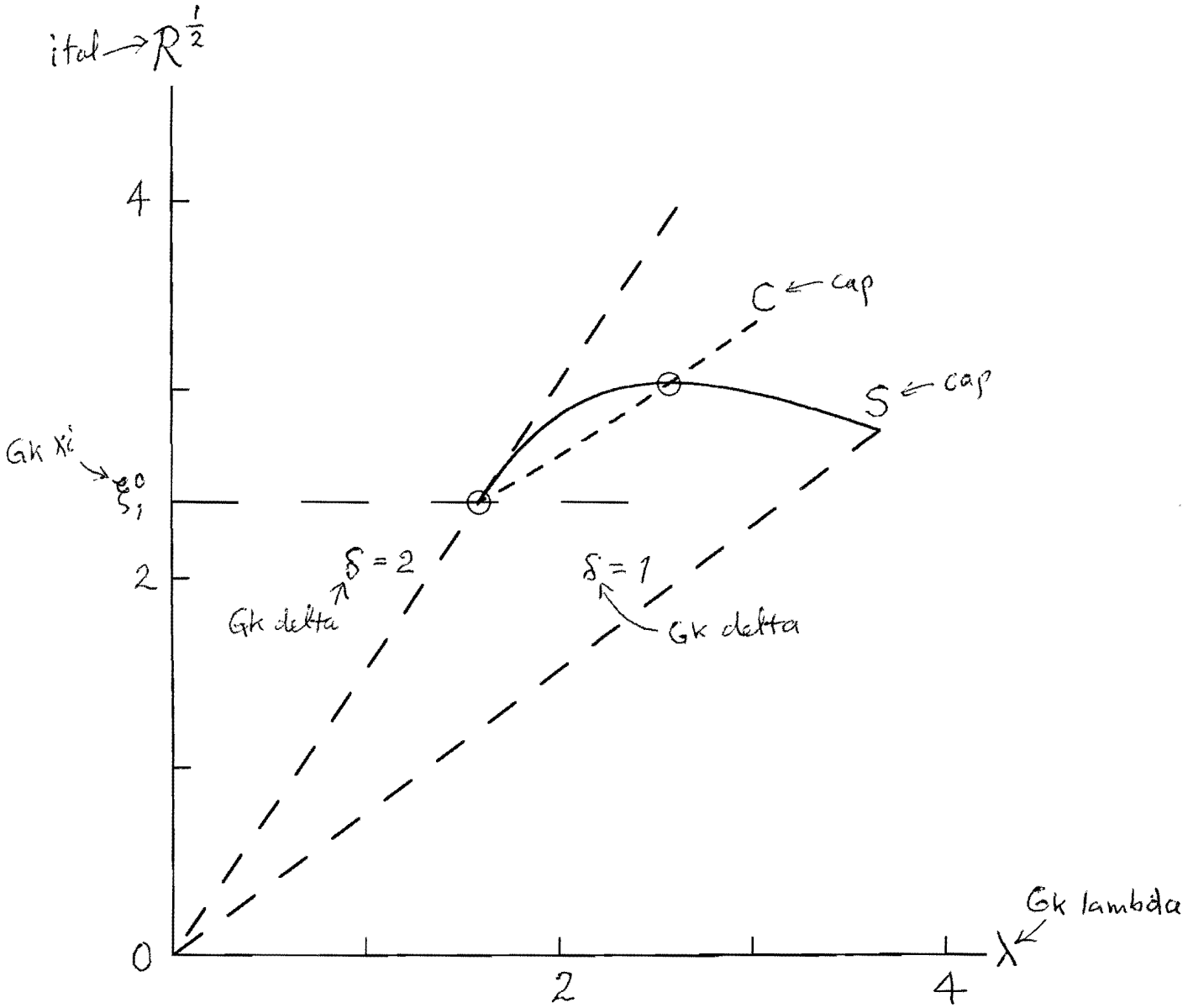

Figure 1. With wavenumber *a* given, curve S shows lower bound for first eigenvalue plotted versus λ ; curve C has been constructed using δ - values satisfying the integral constraint.

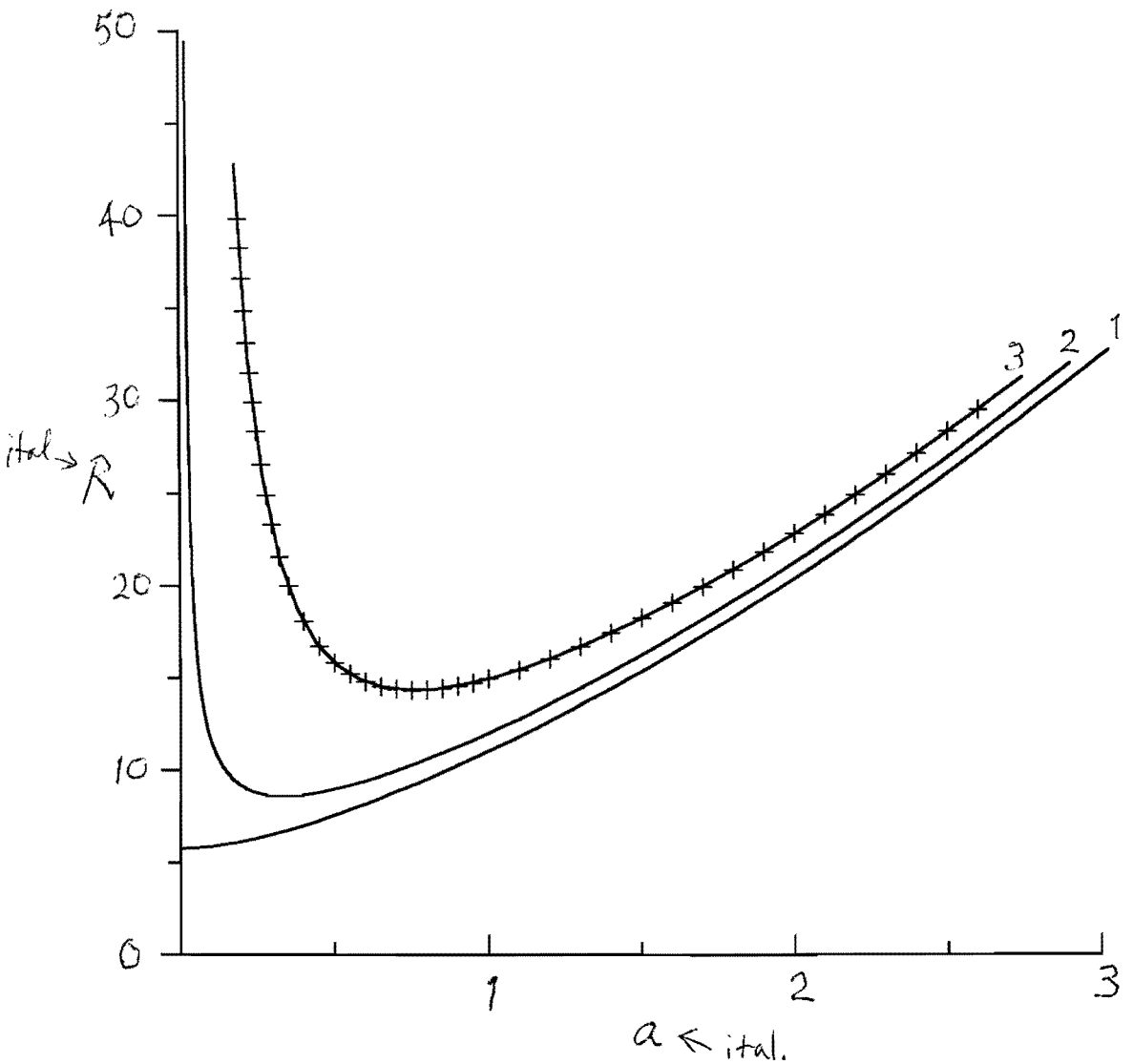

Figure 2. Comparison of estimates involving lowest eigenvalue R_1 versus wavenumber a for the equilibrium boundary layer. Curve 1: Energy method using integral constraint. Curve 2: Energy method using differential constraint. Curve 3: Linearised stability theory using Jacobi-Davidson numerical method (solid curve) and Frobenius expansions (crossed points).

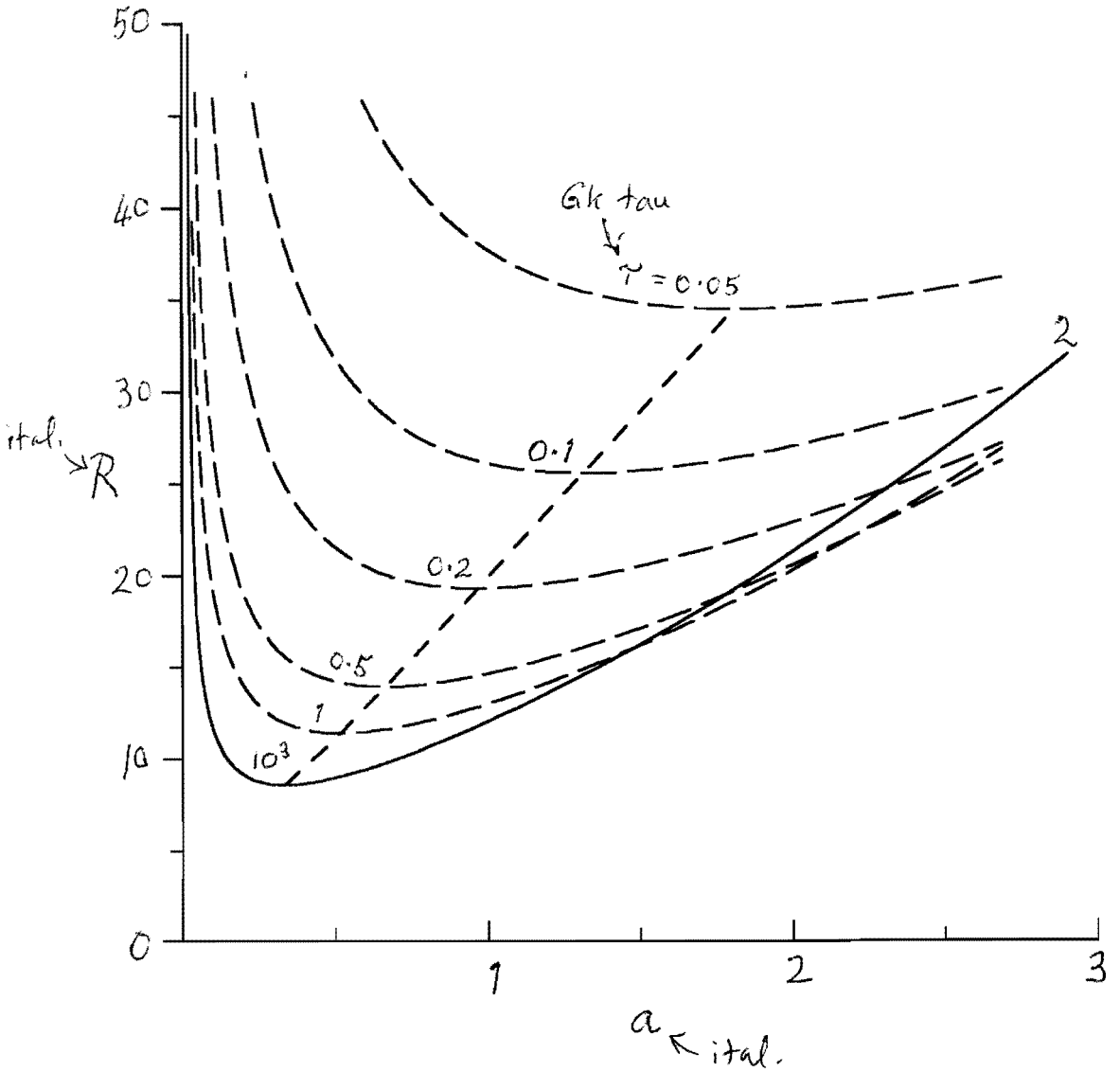

Figure 3. Solid curve: Lower bound to R_1 for equilibrium boundary layer according to the energy method with differential constraint. Dashed curves: Lower bound for R_1 prior to equilibrium. Numerical values are calculated by Jacobi-Davidson method. Short-dashed curve traces minima of lower bound for R_1 with increasing $\tau > 0$.

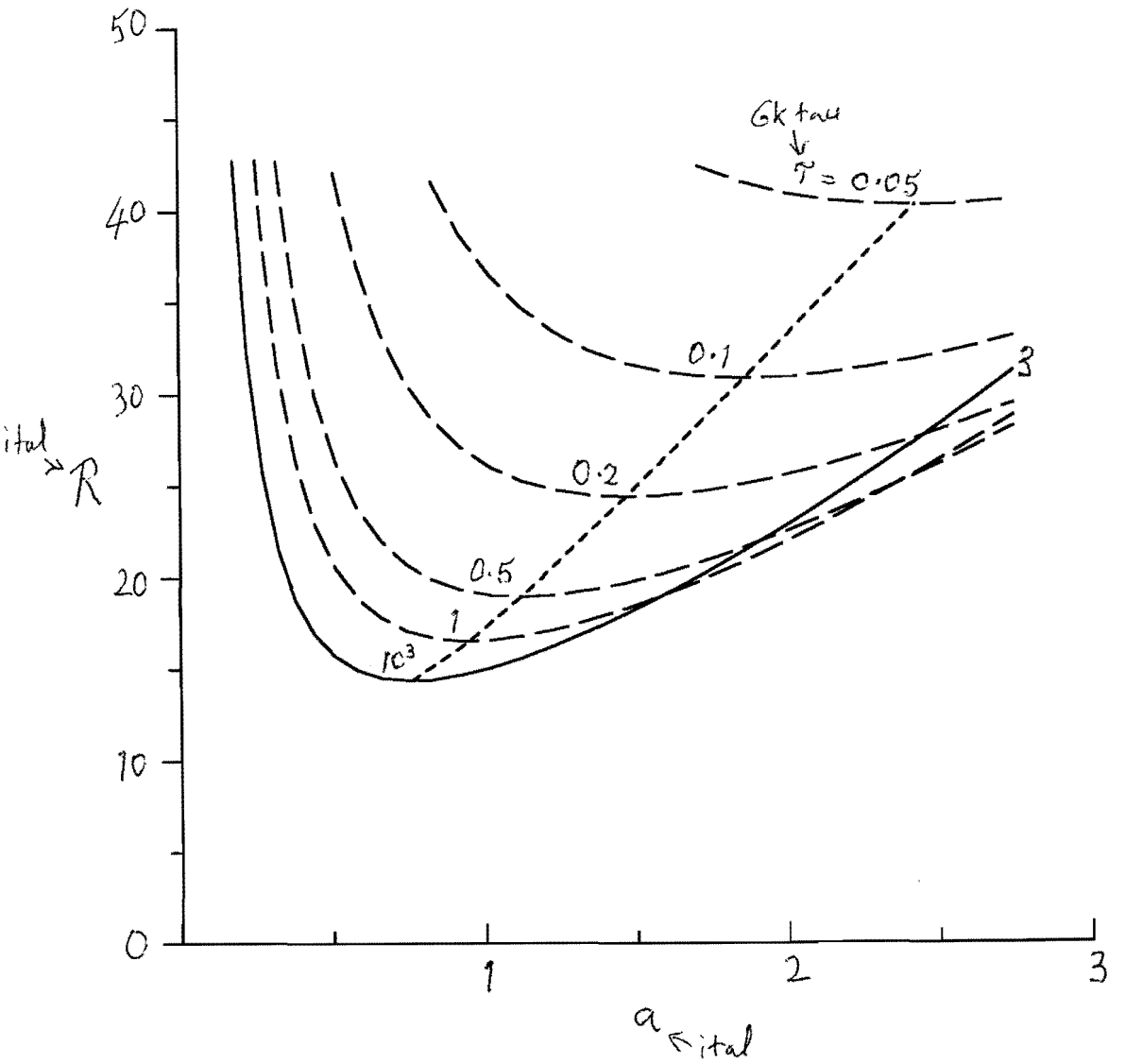

Figure 4. Solid curve: Lowest eigenvalue R_1 for equilibrium boundary layer according to small perturbation theory. Dashed curves: Estimate of R_1 prior to equilibrium, treating time as parameter. Numerical values are calculated by Jacobi-Davidson method. Shorter-dashed curve traces minima of R_1 with increasing $\tau > 0$.

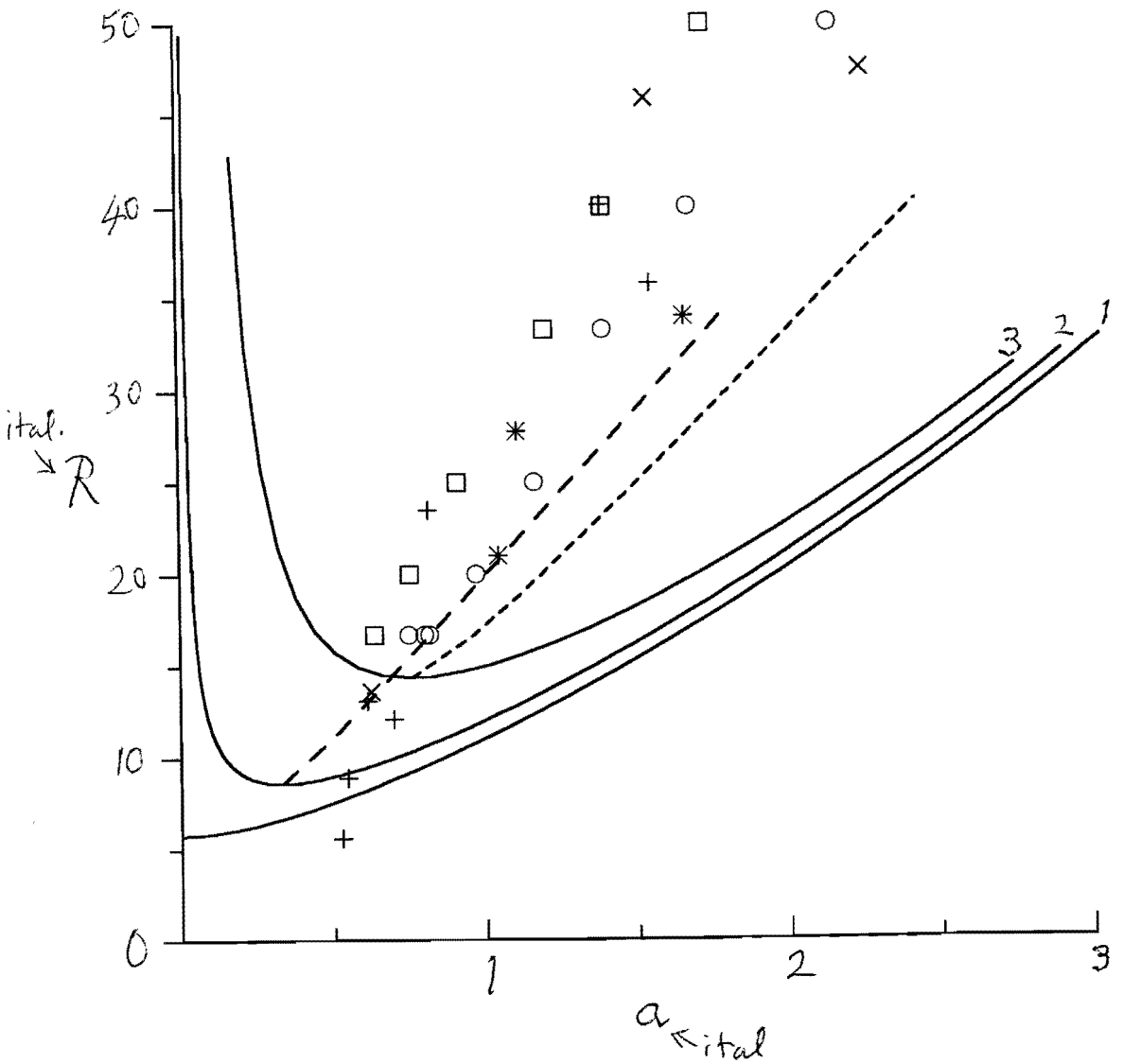

Figure 5. Comparison of theory (this paper) with experimental and numerical modelling results (Wooding, Tyler & White 1997). Solid curves 1-3 give eigenvalues R_1 versus wavenumber a for the equilibrium boundary layer (Figure 2). Curves of minima of R_1 with respect to a for $\tau > 0$ increasing to equilibrium: by modified energy method (Figure 3, short dashes), by linearised theory (Figure 4, shorter dashes). Symbols for experimental and numerical results are identified in the text.

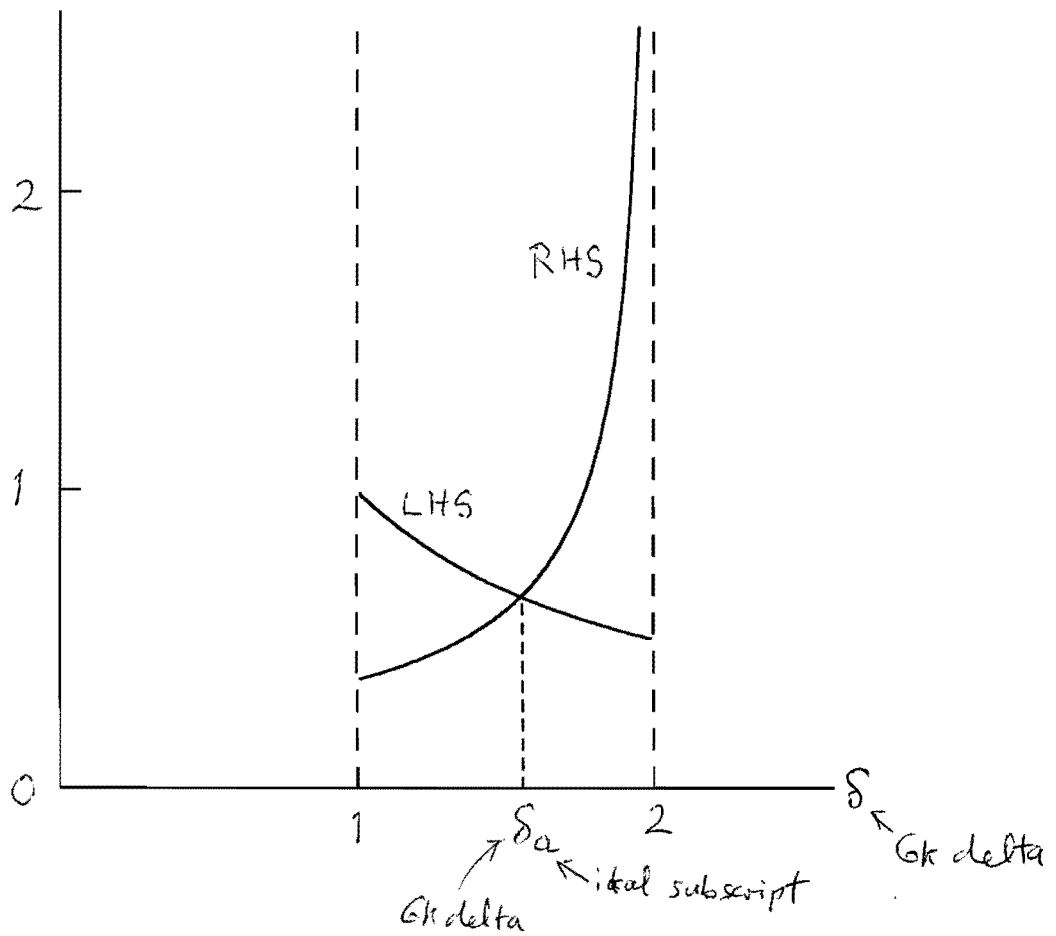

Figure 6. Typical curves of R
likely situation curves are m
uniqueness.